https://doi.org/10.5194/egusphere-2026-3191
Preprint. Discussion started: 12 June 2026

Middle to Late Miocene paleoceanographic evolution of the south-eastern Indian Ocean (ODP Site 752) inferred from nannofossil assemblages

Xabier Puentes-Jorge[1], Arianna V. Del Gaudio[2,1], Werner E. Piller[1], David De Vleeschouwer[2], Tamara Hechemer[1], Gerald Auer[1]

[1]Department of Earth Sciences, University of Graz, NAWI Graz Geocenter, Graz, Austria
[2]Institute of Geology and Paleontology, University of Münster, Münster, Germany

Corresponding author: Xabier Puentes Jorge (xabier.puentes-jorge@uni-graz.at)

Abstract

Understanding how the Earth's system behaves under climate forcing conditions is critical for predicting how future climate change scenarios may affect the planet. In this regard, the Miocene, with an atmospheric temperature ~4°C higher than modern and a near-modern ocean configuration, stands out as a potential analogue for future climate projections. Our current understanding of the Miocene derives principally from the Atlantic and Pacific Oceans, whereas the Indian Ocean remains understudied. Nevertheless, different studies performed in the equatorial Indian Ocean have revealed that the multiple climate shifts that occurred during the Miocene modified both the atmospheric and oceanic processes in this basin (e.g., changes in westerlies position, nutrient flux and productivity). In the present study, we investigate how changes in the climate conditions affected the surface ocean system at Ocean Drilling Program (ODP) Site 752, located in the southeastern Indian Ocean, across the Middle to Late Miocene. For this purpose, we present a new quantitative dataset of calcareous nannofossil assemblages, in conjunction with already existing multi-proxy data.

Our results indicate that the warm atmospheric conditions reached during the Miocene Climatic Optimum (MCO), starting at ~16.9 Ma, caused an intensification of the seasonal signal at ODP Site 752 that lasted until 15.32 Ma. After this period, we detected a shift in the calcareous nannofossil assemblage towards species characteristic of low-nutrient and warm-water conditions (e.g., *Reticulofenestra pseudoumbilicus*, *Reticulofenestra haqii*). Nevertheless, with the progression towards the Late Miocene Cooling, which started at ~7 Ma, and the increased influence of the cooler and more productive Southern Ocean waters, the calcareous nannofossil assemblage evolved into a community characterised by relatively high-nutrient and cold-water taxa (e.g., *Coccolithus pelagicus*, *Calcidiscus leptoporus*). By 10.67 Ma, we recorded a reversion in the nannoplankton assemblage to species typical of low-nutrient and warm-water conditions that lasted until 9.88 Ma. The comparison with available εNd(t) records for Site 752 and 707 (located in the equatorial Indian Ocean) revealed that this change in the assemblage composition responded to a strengthening of the Pacific Ocean water influx occurring at this time. High-nutrient and cold-water conditions were reestablished after 9.88 Ma, lasting until the end of the studied record at ~7.34 Ma. Our evaluation of the primary producer community from a multi-proxy-based perspective revealed a progressive evolution of the surface ocean conditions in the southeastern Indian Ocean region across the Middle to Late Miocene for the first time. Furthermore, the strong correlation with existing proxy data for global climate records suggests that large-scale climate events are the main factors driving the changes in the primary producer community and surface ocean conditions at the Broken Ridge during the Middle to Late Miocene. However, certain regional processes (e.g., strengthening of the Pacific Ocean influx) may also

https://doi.org/10.5194/egusphere-2026-3191
Preprint. Discussion started: 12 June 2026

occasionally influence surface ocean conditions. Moreover, this multi-proxy approach allowed us to better understand the Indian Ocean–Southern Ocean interaction, and more specifically, the nutrient transport efficiency between these two ocean basins during a climate change scenario. Specifically, our multi-proxy-based dataset revealed that the Antarctic divergence region experienced a northward migration after the MCO, leading to a deep reorganisation of nutrient transport across the surface southeastern Indian Ocean.

1. Introduction

The surface ocean represents a critical region for human socioeconomic activities (Costanza 1999; Koehn et al., 2017; Rayner et al., 2019; Teh et al., 2022; Dankel et al., 2023), serves as a junction for atmospheric-oceanic processes and as a pathway for interbasinal water exchange (Kraus and Businger 1994; Chelton and Xie 2010; Auer et al., 2021). Specifically, the upper ocean realm plays a key role in oceanic productivity and nutrient transport between different oceanic areas (Mahadevan and Archer 2000; Williams and Follows 2003; Whitney et al., 2005). The physicochemical conditions of surface layers are susceptible to climatic variations and provide relevant insights into atmosphere-ocean feedback mechanisms (Garcia-Soto et al., 2021; Wang and Gligorovski, 2025). This is crucial for understanding and projecting how ocean environments will be affected by ongoing modern-day climate change.

Shifts in climate conditions can trigger changes in surface ocean ecology through variations in environmental conditions, nutrient availability, and planktonic community structure (Stenseth et al., 2002; Moore et al., 2018; Auer et al., 2023). The plankton assemblage composition is a key element of the ocean biological pump, serving as a tool for nutrient export (including carbon) into the deep ocean (Hauck et al., 2015; Laufkötter et al., 2016). However, the efficiency of this process is affected by the metabolic rates of each species and by local-to-global changes in primary productivity (Laufkötter et al., 2016). In this regard, different studies hypothesise that climate change could lead to a decline in the primary producer's biodiversity, favouring species with lower export efficiency. Furthermore, Moore et al. (2018) showed that sustained climate warming has already decreased ocean primary productivity and nutrient export from pre-industrial levels, and hypothesised that this will be further exacerbated by 2300 due to ongoing climate warming. This will therefore lead to global-scale nutrient redistribution, driven by changes in surface ocean biodiversity, nutrient export efficiency, and primary productivity (Laufkötter and Gruber 2018; Moore et al., 2018).

Multiple studies focused on uncovering how the Earth system behaved during different geological periods to reconstruct potential future climatic conditions (Burke et al., 2018; Püttman and Mutterlose 2021; Kageyama et al., 2024; Tierney et al., 2025). However, the most studied periods are either too cold (Pleistocene) or display a completely different continental configuration (Eocene) compared to future projected scenarios (Henry and Vallis 2022; Burton et al., 2025). In this regard, the Miocene represents an ideal paleolaboratory to study the relationship between climate change and Earth's forcing mechanisms. First, due to the similarities in atmospheric temperature with predicted future scenarios within the frame of the Representative Concentration Pathway projections (~4°C warmer during the Miocene than modern times; Steinthorsdottir et al., 2021). And second, because during the Miocene, the main oceanic basins, and in particular the Indian Ocean, had reached a near-modern configuration (Hamon et al., 2013; Bialik et al., 2019; Steinthorsdottir et al., 2021).

During the Miocene, the Earth system experienced a series of climatic events, which strongly affected global conditions (Steinthorsdottir et al., 2021). One of the best-known events is the

https://doi.org/10.5194/egusphere-2026-3191
Preprint. Discussion started: 12 June 2026

Miocene Climatic Optimum (MCO; ~16.9 – 14.7 Ma; Steinthorsdottir et al., 2021), characterised by moderate to high levels of pCO_2 and elevated atmospheric and oceanic temperatures (up to ~7 – 8 °C above modern day values; Steinthorsdottir et al., 2021). For this reason, the MCO has been the focus of multiple studies and an analogue for future climate model reconstructions (Steinthorsdottir et al., 2020; Holbourn et al., 2022). After the MCO, the Earth experienced a cooling known as the Middle Miocene Climatic Transition (MMCT; 14.7 – 13.8 Ma; Steinthorsdottir et al., 2021). This trend, although less intense, persisted after the MMCT, leading to a progressive global decrease in temperature that culminated in the Late Miocene Cooling (LMC), at ~7 Ma (Herbert et al., 2016; Steinthorsdottir et al., 2021). Previous studies conducted in the Atlantic and Pacific Oceans focused on understanding global climate during the Miocene (e.g., pCO_2, and atmospheric temperature; Super et al., 2018; Fox et al., 2021). However, the Indian Ocean remains overall understudied during the Miocene, with data primarily restricted to low-latitude regions of the Northern Hemisphere (e.g., Betzler et al., 2018; Bialik et al., 2019, 2020; Auer et al., 2023), although some studies have also been conducted at high-latitudes (Majewski 2002; Verducci et al., 2009; Groeneveld et al., 2017). Furthermore, most available data for the Indian Ocean span the Early Miocene to the end of the MCO, excluding the cooling transition that followed (Chakraborty et al., 2018; Sosdian and Lear 2020; Martinot et al., 2022).

The present study aims to reconstruct the evolution of the nannoplankton community and surface ocean conditions across Middle to Late Miocene climatic events in the south-eastern Indian Ocean. Our work thus seeks to uncover the relation between climatic, atmospheric, and oceanic processes during this critical time interval, and how their interactions may affect marine ecosystems in the surface ocean.

1.2 Broken Ridge oceanography

1.2.1 Surface water conditions

Today, surface waters in the Broken Ridge (BR) region are principally characterised by the presence of the West Australian Current (WAC), a temperate (~20-24°C) and nutrient rich current (Álvarez et al., 2011) which results from the progressive mixing between the warm waters of the Agulhas Return Current (ARC), the South Indian Ocean Current (SIOC) and the Antarctic Circumpolar Current (ACC; Figure 1) (Wyrtki 1973; Stramma 1992; Sparrow and Heywood 1996; Stramma and Lutjeharms 1997; Palastanga et al., 2007; Schott et al., 2009). Thus, the mixing intensity between the above-mentioned water masses controls the temperature and nutrient availability of the WAC. Furthermore, the location where mixing occurs also plays an important role in determining the variations of these two parameters (Phillips et al., 2021).

https://doi.org/10.5194/egusphere-2026-3191
Preprint. Discussion started: 12 June 2026

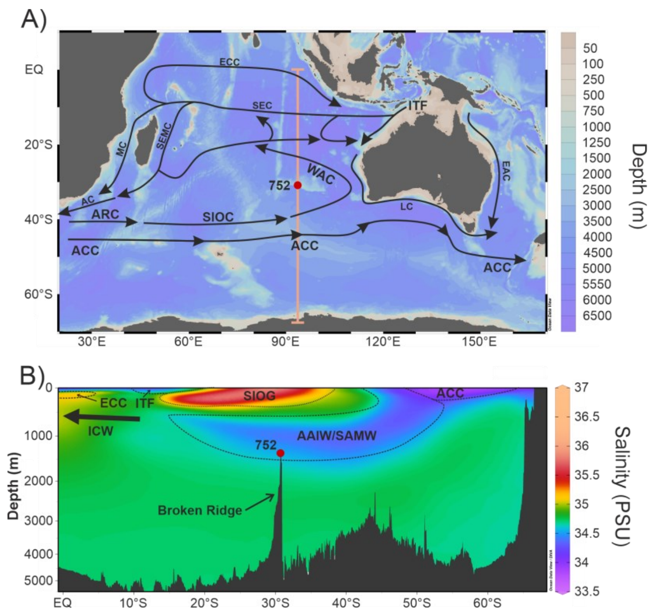

Figure 1: A) paleobathymetric map showing the location of ODP Site 752 (red dot) and surface currents in the Indian Ocean (black lines). The orange line indicates the transect used to generate the salinity profile. B) cross-section showing the salinity profile generated for the Indian Ocean across ODP Site 752. Intermediate and deep currents are identified based on their salinity signature, outlined with a dashed line and labelled accordingly. The paleobathymetric map was generated using Ocean Data View (Schlitzer, 2024), and the salinity data are derived from the World Ocean Database 2023 (Reagan et al., 2024). Abbreviations are as follows: Agulhas Current (AC); Agulhas Return Current (ARC); Antarctic Circumpolar Current (ACC); Antarctic Intermediate Water (AAIW); East Australian Current (EAC); Indian Central Water (ICW); Indonesian Throughflow (ITF); Equatorial Central Current (ECC); Leuwin Current (LC); Mozambique Current (MC); South East Madagascar Current (SEMC); South Equatorial Current (SEC); Southern Indian Ocean Current (SIOC); Southern Indian Ocean Gyre (SIOG); Subantarctic Mode Water (SAMW); West Australian Current (WAC).

1.2.2 Intermediate water conditions

Intermediate waters in the BR area are characterised by the dominance of the Antarctic Intermediate Waters (AAIW) and the Subantarctic Mode Water (SAMW). However, these two water masses flow at slightly different depths. Specifically, the AAIW occupies the deepest portion of the intermediate water layers (700-1300 m), while the SAMW occupies the shallowest (300-700 m; Wong et al., 1999; Hartin et al., 2013). In this context, the shallow SAMW can interact with the surface waters and, in turn, facilitate the exchange of physical and chemical properties between intermediate and surface waters (Harms et al., 2019).

In the IO, the SAMW forms on the equatorward side of the ACC, just south of Australia (primarily during winter) due to heat loss and northward fluxes of cool, low-salinity surface waters from the ACC (Rintoul and England 2002). These two processes intensify convection within the mixed layer, resulting in thicker layers with uniform density and low potential vorticity (relation between absolute vorticity and depth; McCartney 1977). The newly formed

https://doi.org/10.5194/egusphere-2026-3191
Preprint. Discussion started: 12 June 2026

SAMW flows from the Tasman Region toward the Indian Ocean Subtropical Gyre (crossing the BR) and, due to its physicochemical properties, is advected into the thermocline region (Sloyan and Rintoul 2001). This advection ventilates thermocline waters and introduces nutrients into the surface layers, particularly during periods of strong mixing (McCartney 1982; Hanawa and Talley 2001; Li et al., 2022).

2 Material and methods

The analysed samples used in this study were obtained during ODP Leg 121, at ODP Site 752 Hole A (30° 53.475ˈS/93° 34.652ˈE), with a total of 217.32 m of core retrieved (68% recovery). Recovery within the studied interval was 94.7%. The subsequent onboard description revealed two central lithostratigraphic units at ODP Site 752: Unit I (0-113 mbsf) spans from the Pleistocene to the upper Eocene, and it is characterized by foraminifer-nannofossil oozes; Unit II (113-308 mbsf) ranges from the lower Eocene to the upper Maastrichtian, and corresponds to nannofossil chalk with silica-rich layers. We use the astronomically-tuned age-depth model published by Lyu et al. (2023), the accuracy of which was subsequently validated by biostratigraphic data from Puentes-Jorge et al. (2025).

2.1 Quantitative calcareous nannofossil data

132 samples were prepared for quantitative calcareous nannofossil analyses following the methodology outlined in Bordiga et al. (2015). For the slide examination, a standard light microscope (Zeiss Axio Lab.A1), with a field of view (FOV) of 220 µm (22/10X objective; 100X magnification), was used. Calcareous nannofossil specimens were counted based on 2 transects (1/3 and 2/3 of the slide length) of 24 FOV each. To ensure the assemblage was representative of the whole population, additional transects were performed when the total count was lower than 400 counts per sample. On average, ~600 specimens were identified per slide.

2.2 Taxonomic remarks

The taxonomic identification of calcareous nannofossils performed in this study relies on the Handbook of Cenozoic Calcareous Nannoplankton, Volumes 1-5 (Aubry, 1984, 1988, 1989, 1990, 1999), along with the works from Bukry and Percival (1971), Young (1990, 1998), Bown and Dunkley (2012), Galović and Young (2012), Browning et al. (2017), Boesiger et al. (2017) and Howe (2021). Species of the genus *Reticulofenestra* are divided in the present study based on the central aperture and lith size, following the description from the Nannotax website (Young et al., 2017):

Reticulofenestra minuta: reticulofenestrids <3 µm without a bar spanning an open central area.

Reticulofenestra haqii: reticulofenestrids with a coccolith length of 3-5 µm and an open central area.

Reticulofenestra producta: reticulofenestrids with a coccolith length of 3-5 µm with a closed central area.

Reticulofenestra pseudoumbilicus: reticulofenestrids >5µm with an open central area.

Reticulofenestra perplexa: reticulofenestrids >5µm with a closed central area.

The specimens of *R. pseudoumbilicus* and *R. perplexa* were further divided into large (5-10 µm) and very large (>10 µm) morphotypes during the quantitative study. Furthermore, large specimens were divided into two groups (5-7 µm and 7-10 µm) to fully ascertain reticulofenestrid size variations across the study interval.

2.3 Statistical analysis and cluster ordination

The statistical and ordination methods applied in this study were performed using PAST4 (Version 4.13 released in May 2023; Hammer et al., 2001). The above-mentioned statistical analyses include the estimation of correlation indices (Supplement S1) between the nannofossil taxa and different environmental proxies estimated by XRF elemental ratios (see section 2.4). These include determining dust flux into the region and changes in productivity and export productivity (see subchapter 2.4). Additionally, different diversity indices were calculated for the calcareous nannofossil assemblage (Hammer and Harper, 2006). To proceed with the application of ordination and cluster analyses, only the species with an average abundance >0.5% were considered (Supplement S2). Furthermore, species with biostratigraphic relevance, known to appear or become extinct within the studied interval, were not considered for the cluster division due to a potential bias in the results (Mello and Buzas 1968). For analyses, the percentage data were arcsine-transformed to generate a suitable database for ordination and cluster analyses (Sokal and Rohlf 1995; Hammer and Harper 2006; Auer et al., 2014, 2019, 2023; Bialik et al., 2021). Clustering was performed using the universal paired group method with arithmetic mean (UPGMA), using the Bray-Curtis distance. Subsequently, we applied similarity percentages (SIMPER) analyses (Bray-Curtis distance) to assess the contribution of each taxon to the cluster division. 2-D and 3-D non-metric Multidimensional Scaling (nMDS) was applied to the assemblage record to correlate each cluster with a set of available paleoproxy data from ODP Site 752, and nearby locations (see subchapter 2.4 for details on proxy data). The paleoenvironmental proxy data used in the nMDS method were previously interpolated to ensure a proper fit with the calcareous nannofossil assemblage record.

2.4 Geochemical proxy data

A set of previously published geochemical proxy data (Westerhold et al., 2020; Lyu et al., 2023; De Vleeschouwer et al., 2025) was used in this study, along with the generated paleobiological data, to further validate the variations observed in the assemblage. Global $\delta^{18}O$ and $\delta^{13}C$ records from Westerhold et al. (2020) were used to define variations in global temperature and the oceanic carbon cycle, respectively. We generated a dust flux proxy following the methodology outlined in Kuhn et al. (2015), based on the XRF elemental ratio ln(Fe+Ti+Zr)/(K+Al), to assess possible dust influx at the Broken Ridge. This proxy determines the accumulation of heavy mineral phases enriched in Fe, Ti, and Zr, as opposed to elements typically found in clay minerals (K and Al). Additionally, we evaluated changes in productivity using the Si/Ca ratio and the export productivity formula proposed by Lyu et al. (2023) for ODP Site 752. This formula considers the XRF count data of a series of metallic micronutrients that carry a productivity signal, expressed as 1000 x (Cd+Cu+Ni+Zn+Cr+Br)/Ca. Published εNd(t) values were also considered in this study to untangle variations in the oceanographic configuration of the region, as variations in the εNd(t) signal provide critical information about the origin of the waters present in a region at the time of the sediment deposition (De Vleeschouwer et al., 2025).

https://doi.org/10.5194/egusphere-2026-3191
Preprint. Discussion started: 12 June 2026

3 Results

3.1 Calcareous nannofossil diversity data

Preservation of calcareous nannofossil specimens at ODP Site 752 ranges from moderate to moderately poor. This classification was based on visual evaluation of the samples via light and scanning electron microscopes (see Appendix 1 for preservation examples).

Calcareous nannofossil diversity indices calculated at ODP Site 752 show an average of 27 species per sample (Figure 2). The Shannon Index H' calculated for the studied interval ranges between 3.034 and 1.623 (average = 2.466; mean = 2.472). Dominance values at Site 752 are relatively low, with an average value of 0.13 and a minimum of 0.07. However, an increase in dominance is recorded for the interval between 8.90-8.66 Ma, with a maximum value of 0.44 (average = 0.31), coinciding with an increase in abundance of *R. minuta* (Figure 3). Furthermore, the topmost part of the studied time interval shows a slight increase in dominance, with average values of 0.19 (Figure 2).

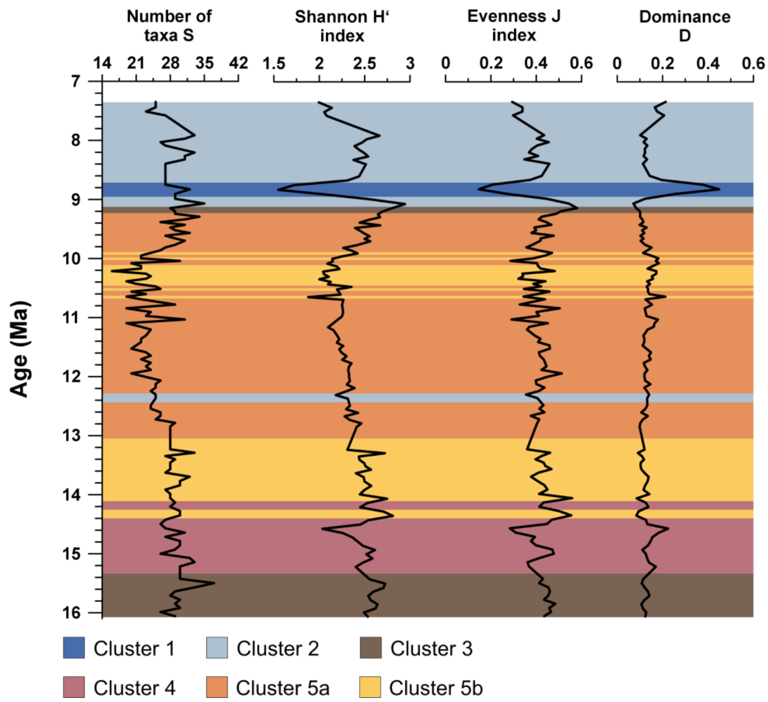

Figure 2: Diversity indices calculated based on the calcareous nannofossil assemblage. All the ecological indices were generated using the PAST4 software (Version 4.13 released in May 2023; Hammer et al., 2001) and includes: Total number of taxa per sample, without considering reworked species; Shannon H' index, calculated following Shannon (1948); Evenness index, calculated as per Buzas and Gibson (1969); Species dominance, calculated as per Simpson (1949). Coloured bands identify the different clusters defined at ODP Site 752.

3.2 Size variations in genus *Reticulofenestra*

Variations in the size of reticulofenestrids were recorded for the interval between 16.1 – 7.34 Ma (Figure 3). In this regard, we considered the difference in abundance between small (<3

https://doi.org/10.5194/egusphere-2026-3191
Preprint. Discussion started: 12 June 2026

μm), medium (3 – 5 μm), large (5 – 10 μm), and very large (>10 μm). Specimens between 5 and 10 μm were considered together due to their similar distribution patterns across the studied interval.

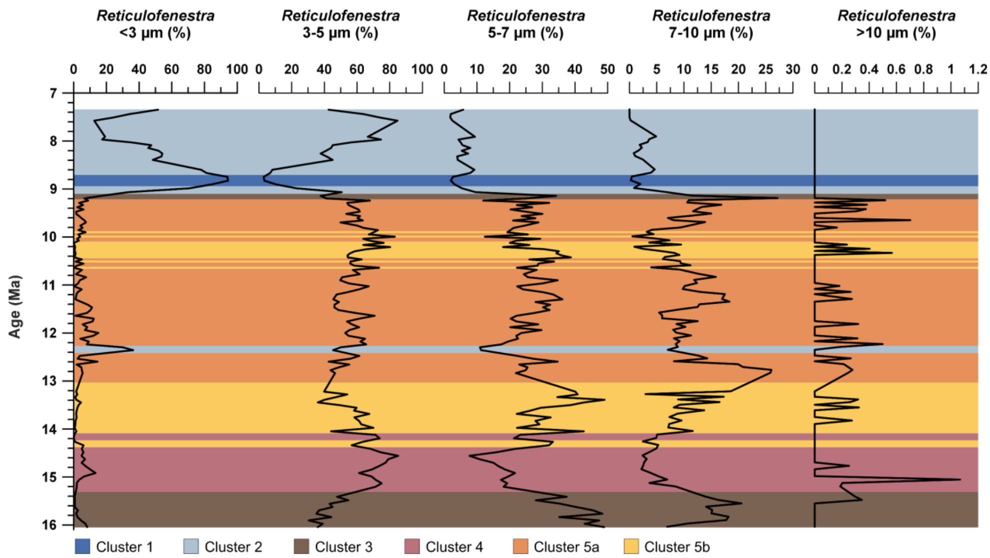

Figure 3: abundance in percentage of the different size range groups of the genus *Reticulofenestra* across the studied interval. Size ranges are divided as defined in Subchapter 2.2, and percentages are rescaled to 100% to allow better comparison between size groups. Clusters are colour-coded.

Mid-size reticulofenestrids generally dominate during the studied interval (55.18%), followed by large-size and small-size reticulofenestrids (32.63% and 12.09%, respectively). Very large reticulofenestrids were very scarce throughout the stratigraphic interval studied (0.08%). Although mid-size reticulofenestrid abundances are higher compared to the other size groups, distinct variations in their relative abundance can be observed throughout the whole studied interval. These variations are usually in concordance with an increase in abundance of large reticulofenestrids (Figure 3). Specifically, large reticulofenestrids exhibit higher abundances in the intervals from 16.1 – 15.32 Ma and 14.09 – 9.22 Ma, followed by a notable decrease in abundance (Figure 3). Remarkably, small reticulofenestrids show a sharp increase in abundance after 9.22 Ma, with abundances rising up to 94 % (Figure 3).

3.3 Cluster ordination and taphogroup characterisation

The clustering ordination analyses performed in this study (UPGMA; Bray-Curtis cophenetic correlation of 0.76) revealed 5 clusters, defined at a cut-off similarity of 0.75 (Figure 4). Furthermore, cluster 5 was divided into two sub-clusters (Subclusters 5a-5b), at a cut-off similarity of ~0.77 (Figure 4). The statistical analyses show a strong similarity in its composition, as per the weak support of individual clusters provided by the bootstrapping (N=1000). However, the p-values obtained from one-way ANOSIM statistics (p-value<0.05) indicate that the clusters defined in this study are statistically significant (Efron and Tibshirani 1994).

https://doi.org/10.5194/egusphere-2026-3191
Preprint. Discussion started: 12 June 2026

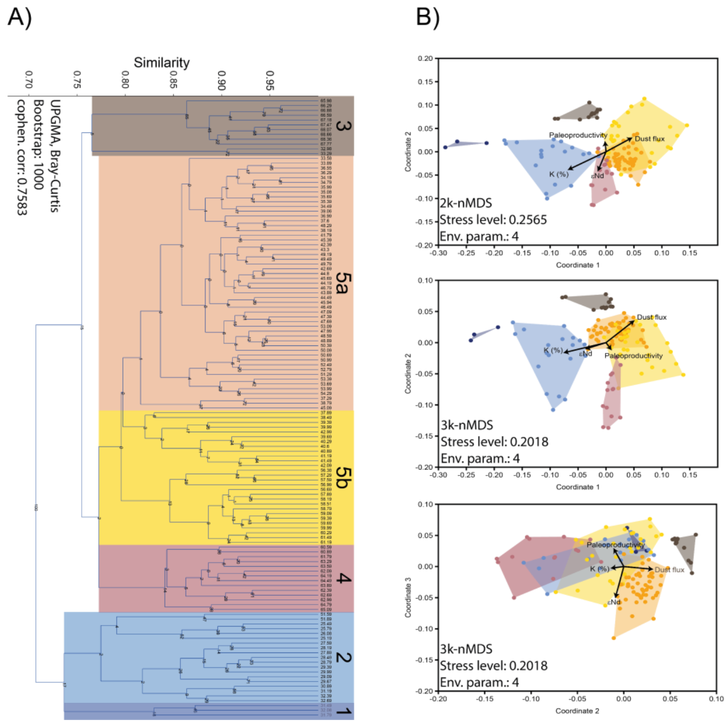

Figure 4: Cluster analyses (A) and nMDS (B) results based on the calcareous nannofossil assemblage shown in Fig. 5.

SIMPER analyses indicate that the clusters and sub-clusters described in this study are defined based on the abundance variability of different reticulofenestrid sizes, discoasterids, *Coccolithus pelagicus,* and *Calcidiscus leptoporus* (Figure 5). Based on the results from the SIMPER analyses, we infer that these clusters are representative of taphogroups, with each reflecting different environmental conditions.

Taphogroup (TG) 1 is characterised by a high abundance of *Reticulofenestra minuta* (64.39 %) and low abundances of medium and large reticulofenestrids (0.92 and 0.83 %, respectively), together with a relatively high abundance of *C. pelagicus* and *C. leptoporus* (5.51 and 7.49 %). TG 2 is also characterised by a relatively high abundance of *R. minuta* (20.91 %). However, TG 2 also presents high abundances of *C. pelagicus* (14.05%) and the highest abundance of *C. leptoporus* (15.70%) from all the TG described at ODP Site 752. TG 3 is defined by a high abundance of *Discoaster* spp. and abundance of *C. pelagicus* (7.38 and 22.56 %, respectively), which are the highest from all the TGs. The abundance of *R. pseudoumbilicus* is also relatively high in this TG (9.03 %). Additionally, *C. leptoporus* shows the lowest abundance in this TG. The TG 4 is characterised by the high abundances of *Reticulofenestra producta* and *Reticulofenestra haqii* (25.56 and 23.42 %, respectively). Finally, TG 5 and the subgroups are distinguished by the increase in abundance of medium and large-sized reticulofenestrids. Specifically, TG 5a presents high abundances of *R. producta*, *R. perplexa,* and *R. pseudoumbilicus* (26.43, 12.72, and 10.93 %, respectively), while TG 5b presents a higher

https://doi.org/10.5194/egusphere-2026-3191
Preprint. Discussion started: 12 June 2026

abundance of *R. haqii* (19.82 %) when compared with TG 5a (7.76%), and a decrease in abundance of *R. perplexa* and *R. producta* (3.83 and 16.05 %).

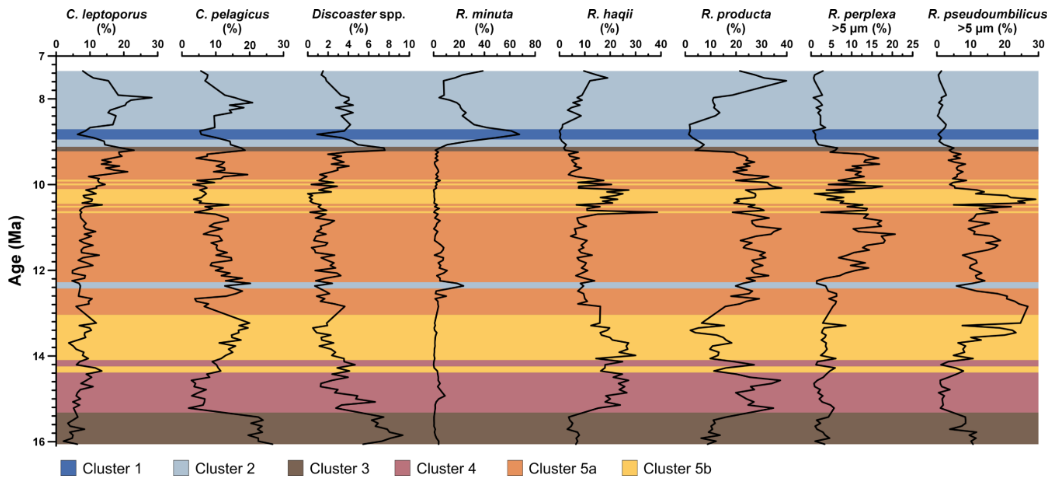

Figure 5: abundance in percentage of the main species defining the cluster division at ODP Site 752 across the studied interval. Clusters are identified by the different colours.

The cluster differentiation is not as evident within the nMDS analyses (Figure 4), where TG 5a and 5b appear grouped. Furthermore, the registered stress level (0.2565 in a k=2; 0.2018 in a k=3) indicates that the plots resulting from the nMDS are difficult to interpret (Clarke 1993). However, Dexter et al. (2018) demonstrated that the degree of stress in the nMDS analyses is positively correlated to the size of sampling. Furthermore, the Bray-Curtis distance index values calculated for the data used in this study show a pattern consistent with the cluster division proposed by the clustering ordination method. Additionally, the one-way ANOSIM (permutations = 9999) test displays p-values <0.05 (sequential Bonferroni significance) for all the cluster and subcluster divisions, which is indicative that the clusters are, indeed, statistically relevant (Somerfield et al., 2021a, 2021b).

4 Discussion

4.1 Environmental significance of the defined taphogroups

***Taphogroup 1* (= cluster 1).** TG 1 is characterised by the bloom of small-sized reticulofenestrids (*R. minuta*), as evidenced by the cluster ordination. This is further supported by the nannofossil diversity indices, which show an increase in dominance (D = 0.34) despite no major variations in the number of taxa (S = 29; Figure 2), compared to the rest of the taphogroups. *R. minuta* is defined as an r-selected species that thrives in high nutrient conditions, and is associated with an increase in the terrigenous influx in coastal areas. However, the position of ODP Site 752 (in an open ocean context; Figure 1) and dust flux estimations (Figure 6) do not align with this hypothesis. Therefore, a new mechanism needs to be invoked to explain the shift in size of the genus *Reticulofenestra*. Different studies hypothesized that nitrogen (N) could play a crucial role in determining the size variations of coccoliths in open ocean settings, leading to a reduction of the coccolith size during intervals where N is limited (Paasche 1998; Aloisi 2015; Auer et al., 2023). Nitrogen limitation in open ocean settings has been correlated to a relative excess of phosphorus in the water (Deutsch

https://doi.org/10.5194/egusphere-2026-3191
Preprint. Discussion started: 12 June 2026

et al., 2007). The increase of phosphorus with respect to the N, also known as "phosphorus excess", produces a variation in the relative Redfield ratio from 106C:16N:1P, leading to the existence of high C and P waters which can not sustain a high biological productivity due to the low N availability (Moore et al., 2008). Additionally, TG 1 also shows relatively high abundances of *C. pelagicus* and *C. leptoporus*, which thrive in cold water regions. Thus, we associate TG 1 with the presence of high-nutrient (N-limited) cold waters in the BR area.

***Taphogroup 2* (=cluster 2).** The TG 2 has a similar species distribution as TG 1, with a high abundance of *R. minuta*, *C. pelagicus,* and *C. leptoporus*, which are indicative of similar oceanic conditions. However, TG 2 presents higher *C. leptoporus* and *C. pelagicus* and lower *R. minuta* abundances than TG 1. This difference in species abundance within TG1 and TG2 is also supported by the diversity indices, which show a lower dominance in this taphogroup (D = 0.15) and a more even species distribution (J_{TG2} = 039; J_{TG1} = 0.21). We link the increase in the cold-water species (and decrease in *R. minuta*) to the persistence of high-nutrient cold waters and an increase in the N-availability in the photic zone in the BR region.

***Taphogroup 3* (=cluster 3).** The TG 3 is defined by the common presence of *Discoaster* spp., *R. pseudoumbilicus* and *C. pelagicus*. Previous studies from Imai et al. (2015) and Tangunan et al. (2018) associated the presence of *Discoaster* spp. and large-sized reticulofenestrids with warm and oligotrophic waters in deep nutricline settings. However, different authors argued that the increase in large-sized reticulofenestrids is, in fact, linked to high nutrient conditions (Auer et al., 2014; 2015; 2023; Beltran et al., 2014). This interpretation is further supported by comparison with modern analogues of the *Reticulofenestra* group (*Gephyrocapsa* spp.), which showed an increase in size under high nutrient conditions (Aloisi 2015). However, these conditions do not explain the abundances observed for *C. pelagicus*, which thrives in well-mixed cold waters (Cachão and Moita 2000; Sato et al., 2004). In this regard, multiple studies have associated the presence of species characterised by opposite ecologies as a signal of seasonality. Specifically, warm and oligotrophic related taxa would be compatible with warm summer periods, which allowed the establishment of a seasonal thermocline and inhibited the nutrient advection in the upper ocean layers. Conversely, cold water taxa would thrive during winter periods, where a deepening of the mix-layer would result in an enhanced nutrient availability. Based on this evidence, we interpret TG 3 as an assemblage reflecting strong seasonality. This interpretation is in agreement with the diversity indices calculated for the TG3, which shows that this taphogroup is the most diverse (S = 30; H' = 2.54) and more evenly distributed (J = 0.45; D = 0.11) among all the taphogroups.

***Taphogroup 4* (=cluster 4).** The TG 4 is characterised by the dominance of medium-sized reticulofenestrids, which have been linked to elevated nutrient conditions (eutrophic to mesotrophic) in warm/temperate areas (Auer et al., 2023; Viganò et al., 2023) and to locally confined upwelling (Wade and Bown, 2006; Auer et al., 2015). These oceanographic conditions are intermediate between those observed for TG1 and TG5. This interpretation is further supported by the diversity indices, which revealed a moderate diverse and evenly distributed nannoplankton community (S = 29; H' = 2.44; D = 0.15; J = 0.4) compared to the assemblages in TG1 and TG5. However, the position of Site 752 (within the subtropical Indian Ocean gyre system) makes it unlikely for these conditions to occur. Therefore, we hypothesize that changes in the nutrient source could, indeed, be the reason for the change in mid-size reticulofenestrid size distribution. This interpretation is further supported by empirical studies in culture, where changes in the Redfield nutrient relation showed an effect on the coccolith

https://doi.org/10.5194/egusphere-2026-3191
Preprint. Discussion started: 12 June 2026

size (Aloisi 2015). Thus, we associate TG 4 with temperate waters characterised by high N and P availability.

***Taphogroup 5a* (=subcluster 5a)**. The TG 5a is defined by the common occurrence of *R. pseudoumbilicus*, linked to high nutrient waters in warm-water areas (Lohmann and Carlson 1981; Auer et al., 2015, 2023; Aloisi 2015), and *R. haqii*, linked to a deep thermocline/nutricline also in relatively warm areas (Wei and Wise 1990; Wade and Bown 2006; Auer et al., 2015, 2023). The correlation of this taphogroup with high nutrient conditions is further supported by the diversity indices, which show the lowest values (S = 25; H' = 2.33) among the all taphogroups. Hence, we link TG 5a to the presence of relatively warm waters and a deep thermocline/nutricline in the BR region.

***Taphogroup 5b* (=subcluster 5b).** The TG 5b is characterised by the concomitant occurrence of large-size reticulofenestrids, linked to high nutrient waters in temperate areas (Lohmann and Carlson 1981; Auer et al., 2015, 2023; Aloisi 2015), and *R. producta*, associated with a deepened thermocline/nutricline (Wei and Wise 1990; Wade and Bown 2006; Auer et al., 2015, 2023). The nannoplankton diversity indices also sustain this hypothesis, with overall low number of taxa (S = 26) and low diversity (H' = 2.36) compared to TG5a. Therefore, we link TG 5b to the presence of relatively cold waters and a deep thermocline/nutricline in the BR region.

4.2 Paleoclimatic control and evolution of paleoceanographic conditions at Broken Ridge

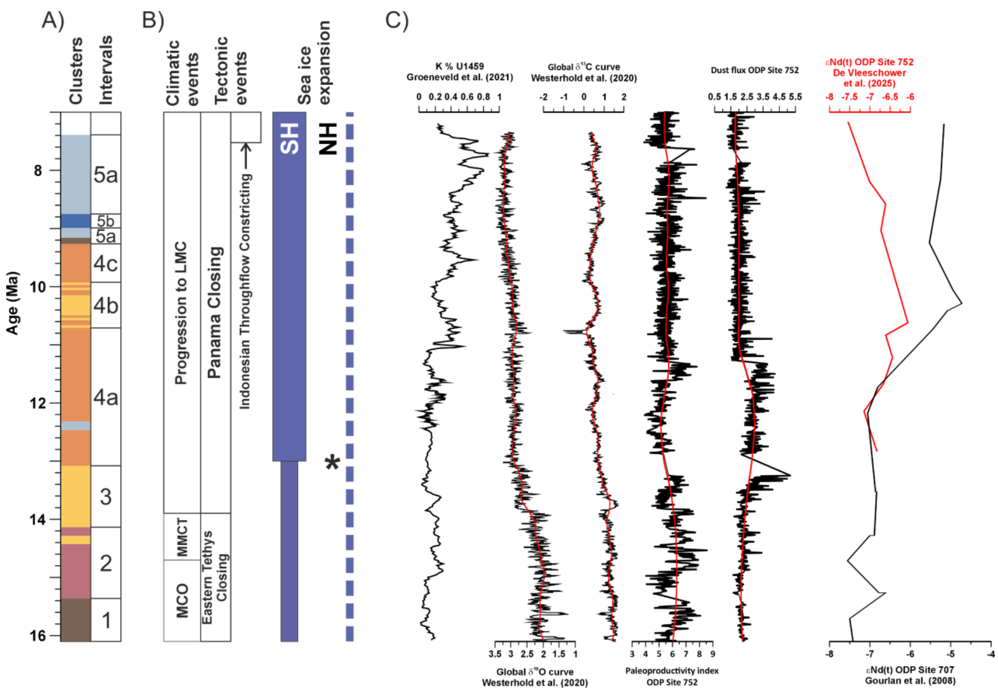

Figure 6: A) representation of the clusters and related intervals defined at ODP Site 752; B) a compilation of global and Indian Ocean major climatic and tectonic events that occurred across the targeted interval (16.1 – 7.34 Ma); The Southern Hemisphere (SH) and Northern Hemisphere (NH) sea ice extension is also included and shows an increase in ice volume after

https://doi.org/10.5194/egusphere-2026-3191
Preprint. Discussion started: 12 June 2026

~13 Ma (*=perennial ice formation in the NH);C) set of global and Indian Ocean specific geochemical data compiled for the studied interval. The $\delta^{18}O_{Benthic}$ megasplice shows stable conditions in deep ocean temperature and ice volume until 13 Ma (Westerhold et al., 2020), while the $\delta^{13}C_{Benthic}$ highlights variations in the C cycle across the studied interval. The $_{\varepsilon}$Nd(t) values show an increase of Pacific Ocean waters between ~10.7-9.9 Ma (De Vleeschouwer et al., 2025), which correlates with the timing of an increase in winnowing (Lyu et al., 2023). The dust flux index shows an increase after ~9.2 Ma (Auer et al., 2023).

Based on the variations observed in the assemblage variability defined by our taphogroups, we could subsequently define a total of 5 intervals (1-5) and 4 subintervals (4a-c and 5a) at the BR region. We interpret these intervals as progressive surface ocean changes of mean nutrient availability, temperature, and water column mixing between 16.1-7.31 Ma. Variations in the assemblage data were compared with a set of geochemical proxies from the global Ocean and the Indian Ocean (Westerhold et al., 2020; Lyu et al., 2023; De Vleeschouwer et al., 2025) to ascertain the paleoceanographic and climatic conditions that occurred during these intervals (Figure 7A-C). The identified intervals, along with their paleoceanographic and climatic implications, are detailed in the following paragraphs.

Interval 1 (base of the studied interval -15.32 Ma): Interval 1 is defined solely by TG 3, which is characterised by a mixed assemblage with abundant *R. pseudoumbilicus*, *C. pelagicus,* and *Discoaster* spp. This interval presents an average number of taxa of 30±3 (N=10), with an average diversity index (Shannon H' index) of 2.60±0.08 and a dominance index of 0.11±0.01.

Interval 2 (15.32-14.09 Ma): Interval 2 is distinguished by the continuous presence of TG 4, which intercalates with TG 5a at the top of this unit. The interval is characterised by a calcareous nannofossil assemblage with abundant mid-size reticulofenestrids (TG 4), which decrease in abundance when TG 5a is present, being replaced by larger *Reticulofenestra* species. Additionally, a drop in the abundance of *C. pelagicus* can be observed at the bottom of interval 2, reflecting the switch from TG3 to TG4. Diversity indices calculated for this interval show an average number of taxa of 29±2 (N=16), a Shannon H' index of 2.48±0.1,8, and a dominance of 0.14±0.03.

Interval 3 (14.09-13.04 Ma): Interval 3 is characterised solely by TG 5a, which reflects common *R. pseudoumbilicus* and mid-size reticulofenestrids. *Reticulofenestra pseudoumbilicus* exhibits an increasing trend, whereas mid-size reticulofenestrids decrease through interval 3. This period shows an average number of taxa of 29±2 taxa (N=14), with a Shannon H' index of 2.51±0.12 and a dominance index of 0.12±0.02.

Interval 4a (13.04-10.67 Ma): Interval 4 is distinguished by TG 5b, with a brief interval characterised by TG 2. Here, we observe an assemblage dominated by *R. perplexa*, concomitant with a high abundance of *R. producta*. This interval presents an average of 24±3 (N=35) taxa, with a Shannon H' index of 2.28±0.08 and a dominance of 0.15±0.02.

Interval 4b (10.67-9.88 Ma): Interval 4a is characterised by the alternation between TG 5a and 5b, mainly ruled by the variations in abundance of *R. perplexa*. The average number of species during this interval is 29.00±2 (N=18), with a Shannon H' index of 2.57±0.06 and a dominance index of 0.11±0.01.

Interval 4c (9.88-9.22 Ma): Interval 4c is characterised solely by TG 5b and, therefore, with similar conditions to those recorded during intervals 4a and b (see discussion above).

https://doi.org/10.5194/egusphere-2026-3191
Preprint. Discussion started: 12 June 2026

However, diversity indices show slightly different values, with an average of 29.00±2 (N=14) taxa, a Shannon H' index of 2.50±0.12, and a dominance index of 0.13±0.02.

Interval 5a (9.22-top of the studied interval): Interval 5a is characterised by the presence of TG 2, TG 3, and a small subinterval (Interval 5b) characterised by TG 1 (see detailed discussion below). The change from interval 4c to 5a is marked by a sharp decrease in the abundance of mid- to large-sized reticulofenestrids and the increase of *Discoaster* spp., *C. leptoporus,* and *C. pelagicus*. These changes in the planktonic assemblage remain relatively stable through interval 5a, except for *Discoaster* spp., which is only abundant when TG 3 is recorded. Diversity indices show an average of 29.00±3 number of taxa, a Shannon H index of 2.35±0.34, and a dominance index of 0.10±0.1.

Interval 5b (8.95-8.71 Ma): Interval 5b is comprised within a narrow period in interval 5a, which is characterised exclusively by TG 1, where *R. minuta* is dominant. Diversity indices show an average of 29.00±3 (N=3) taxa, a low Shannon H' index (1.78±0.26), and high dominance (0.37±0.1) during this interval.

The five intervals established at ODP Site 752 reflect a dynamism of the region, susceptible to multiple oceanic factors. Specifically, based on the variations of the calcareous nannofossil assemblage, we infer that only the combined influence of water temperature, stratification, and nutrient availability can explain changes in paleoecological conditions on the Broken Ridge (BR) over the Middle to Late Miocene (~16.1 – 7.31 Ma). Our data suggest that the BR was dominated by seasonal conditions during Interval 1, as per the presence of nannoplankton species with opposed ecological niches (e.g., *C. pelagicus* and *Discoaster* spp.; Auer et al., 2023). In this regard, multiple studies observed a positive relation between the seasonal signal and global high temperatures (e.g., Klotz et al., 2006; Jo et al., 2022). Here, we link our observations to the elevated global temperatures recorded during the MCO (Steinsthordottir et al., 2021), which could, in turn, lead to a strong contrast between austral summer/winter conditions (Figure 7A). These higher temperatures are further supported by the global benthic foraminifera $\delta^{18}O$ isotopic stack, which shows values ranging between ~1.5 to ~2.25 ‰ for this period (Figure 6; Westerhold et al., 2020).

A shift towards cooler and more nutrient-enriched waters, as well as a deepening of the thermocline/nutricline and a reduction in seasonality, is presumed during Interval 2. We ascribe the change in the nannofossil assemblage and paleoceanographic conditions to a progressive global evolution from the MCO to the MMCT, which occurred during this period (Figure 6). This interpretation also aligns with benthic foraminifera $\delta^{13}C$ and $\delta^{18}O$ isotopic data (Westerhold et al., 2020), which reveal a positive shift in their values in correspondence to Interval 2 (Figure 6). Our results demonstrate that persistent cool and nutrient-rich surface water conditions were achieved at approximately 14.09 Ma at the Broken Ridge (beginning of Interval 3), close to the end of the MMCT (~13.9 Ma). This cooling trend persisted through intervals 3 and 4a (Figure 7B). This interpretation aligns with global $\delta^{18}O$ records, which show values ranging from 3.26‰ to 1.76‰ (Figure 6). Moreover, our assemblage data also suggest the presence of slightly colder waters during Interval 4a at the Broken Ridge.

A change in the calcareous nannofossil assemblage was detected at 10.67 Ma. This shift in the assemblage composition occurs concomitantly with a positive excursion in the $_{\varepsilon}$Nd(t) values recorded at ODP Site 752, which was recently correlated with an increase in the Pacific Ocean water input to the region in De Vleeschouwer et al. (2025). Furthermore, the global $\delta^{13}C$ signal

https://doi.org/10.5194/egusphere-2026-3191
Preprint. Discussion started: 12 June 2026

also shows an increasing trend during this period (Figure 6), which was ascribed to variations in the global C cycle and nutrient availability in the surface ocean (De Vleeschouwer et al., 2020). We ascribe these variations to a decrease in the nutrient availability and an increase in the temperature due to the enhanced input of warm Pacific Ocean waters. These conditions remain consistent until the end of Interval 5, at 9.88 Ma, before continue a cooling trend until the end of our record at ~7.34 Ma (end of Interval 5; Figure 7C). Interestingly, we recorded an increase in the abundance of *R. minuta* at ODP Site 752 between 8.95 – 8.71 Ma, in synchrony with other contemporary records (Haq 1980; Young et al., 1998; Krammer et al., 2006; Beltran et al., 2014; Imai et al., 2015; Auer et al., 2023). Specifically, the calculated diversity indices indicate that, during this period, *R. minuta* replaces most of the calcareous nannofossil assemblage taxa (Figure 2). Different studies have linked the increase of small reticulofenestrids to changes in the nutrient cycle (Båtvik et al., 1997; Paasche, 1998; Müller et al., 2008; Aloisi, 2015; Langer et al., 2023). However, no variations in the global $\delta^{13}C$ are observable during this period (Figure 6). However, different authors highlighted the key role of the N:P ratio in determining the size distribution of modern reticulofenestrids (Marañon et al., 2013; Aloisi, 2015). Specifically, in-lab experiments show that N-limitation in nutrient-enriched environments can lead to a significant decrease in the coccolith size. Thus, we propose that the increase in abundance of *R. minuta* is related to a change in the N cycle, leading to a decrease in the N availability at ODP Site 752.

https://doi.org/10.5194/egusphere-2026-3191
Preprint. Discussion started: 12 June 2026

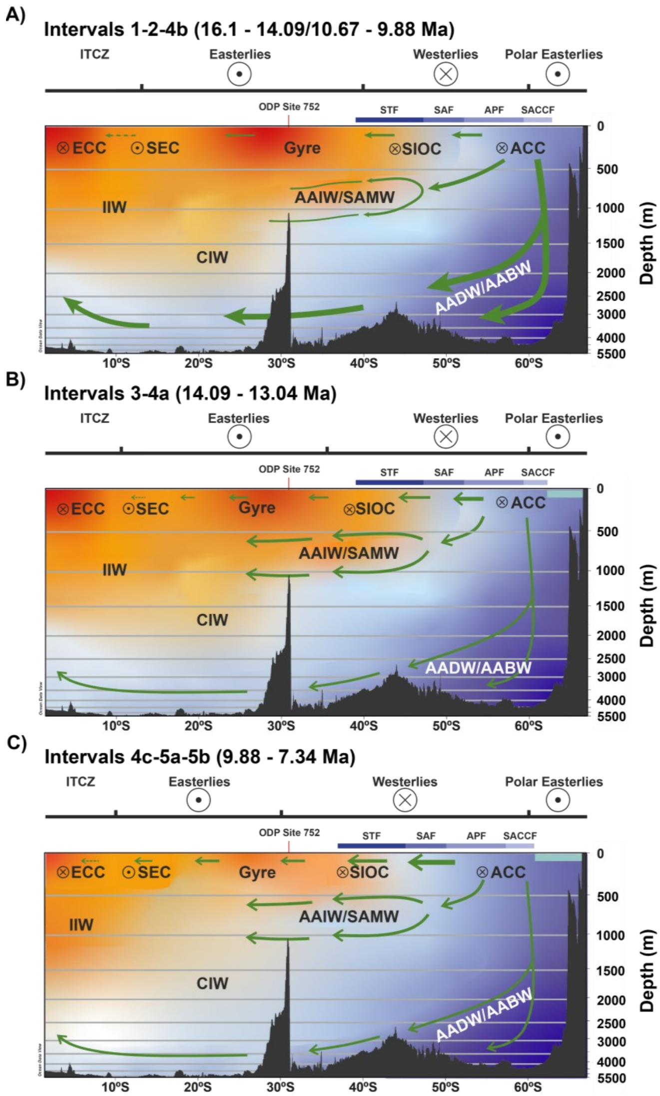

Figure 7: conceptual model of the paleoceanographic evolution between Antarctica and the Equatorial Indian Ocean across ODP Site 752 through the study interval (16.1 – 7.34 Ma). Water relative temperature is represented by the blue (cold) to red (warm) gradient. Furthermore, changes in the transport of nutrients across the Indian Ocean basin are highlighted by the thickness of the green arrows (thicker arrow=higher nutrient transport). The position of the zonal wind conveyor belts for the three presented scenarios is extrapolated from Groeneveld et al. (2017). The polar front system and sea ice extension represent their hypothesised migration under the paleoceanographic conditions inferred in this study. The paleobathymetric profile was generated using Ocean Data View (Schlitzer, 2024). Additionally, literature data (You 1998; Böning and Bard 2009; Auer et al., 2023; De Vleeschouwer et al., 2025) were considered to better adapt the variations in the paleoceanographic conditions across the selected transect. Abbreviations are as follows: Antarctic Bottom Water (AABW);

https://doi.org/10.5194/egusphere-2026-3191
Preprint. Discussion started: 12 June 2026

Antarctic Circumpolar Current (ACC); Antarctic Deep Water (AADW); Antarctic Intermediate Water (AAIW); Antarctic Polar Front (APF); Central Indian Water (CIW); Indian Central Water (ICW); Equatorial Central Current (ECC); Indian Intermediate Water (IIW); Intertropical Convergence Zone (ITCZ); South Equatorial Current (SEC); Southern Indian Ocean Current (SIOC); Southern Indian Ocean Gyre (SIOG); Subantarctic Circumpolar Current Front (SACCF); Subantarctic Front; Subantarctic Mode Water (SAMW); Subtropical Front (STF).

4.3 Variations in the mid-latitude surface Indian Ocean nutrient pool and Antarctic nutrient transport

Substantial variations in the nutricline depth and surface ocean nutrient content can be inferred through the 5 intervals defined at ODP Site 752. According to the calcareous nannofossil data, we can hypothesise that these changes in the nutrient cycle are linked to two main factors: 1) changes in the nutrient availability due to variations in the nutrient transport (William and Follows 2003; Sarmiento et al., 2004; Moore et al., 2013). 2) changes in the nutrient composition via intensification of the organic matter degradation in the water column, also known as remineralisation (Lefèvre et al., 1996; Feely et al., 2004). Here, we explore in detail how factor 1 could potentially affect the nutrient availability in the surface ocean during the Middle to Late Miocene. Nutrients are transported into the Broken Ridge area via the Tasman Leakage or the Antarctic divergence region in the modern ocean (Koch-Larrouy et al., 2010; Lyu et al., 2023; Bali et al., 2025). However, Lyu et al. (2023) established the onset of the Tasman Leakage during the Late Miocene, at 7 Ma, although some sporadic occurrences of the Tasman Leakage could occur between 10.8-7.5 Ma. Therefore, we consider the nutrient supply in the Broken Ridge region intrinsically connected to the dynamics of Antarctic divergence during our study interval.

Between 16.1 – 15.32 Ma, we observe a variation in the depth of the nutricline at the Broken Ridge area, linked to the summer/winter contrast. Specifically, we infer a deepening of the nutricline during winter and a shoaling during summer, driven by thermocline variability in a warmer MCO world (Figure 7A). In this regard, we ascribe the high nutrient-related species to the winter periods, where strong mixing produced the nutrient elevation into the photic zone. Conversely, summer conditions are typically marked by reduced nutrient concentrations in the upper water column. Our hypothesis suggests that surface nutrient lateral transport into the BR region remains limited during the whole interval between 16.1-15.32 Ma. However, during winter periods, the studied area can go through nutrient enrichment due to the expansion of the mixed layer and the subsequent incorporation of intermediate waters. This scenario is compatible with a very southern position of the Antarctic divergence, where surface nutrients are slowly consumed before arriving at the Broken Ridge. Although nutrient conditions remained relatively low during this period at ODP Site 752, the productivity index shows the highest values here. We hypothesise that this increment in productivity might be related to an increase in the nannoplankton metabolic ratio as a consequence of the higher sea surface temperatures experienced during the MCO.

After 15.32 Ma, we observe a continuous deepening of the nutricline at Site 752, accompanied by an increase in the nutrient conditions that lasts until 10.67 Ma. This is further supported by a decrease in diversity of the nannofossil assemblage, which is commonly related to an increase in nutrient availability (Hallock 1987; Figure 2). The increase in the surface ocean nutrient content is indicative of an enhanced lateral transport from the Antarctic region, which is, ultimately, related to a northward shift of the downwelling region (Figure 7A-B). A decrease

https://doi.org/10.5194/egusphere-2026-3191
Preprint. Discussion started: 12 June 2026

in the productivity index accompanies the progressive increase in nutrient availability between 15.32 and 10.67 Ma. However, this decrease is also coeval with a reduction in the δ^{18}O during this period, further supporting the hypothesis that productivity in the region is ruled by ocean temperature rather than nutrient availability. Smaller-scale variations in the nutrient availability can be identified during this time. Nevertheless, these variations are likely related to local variations in the oceanographic regime, and not to the occurrence of large-scale processes ruling nutrient transport in the region (see subchapter 4.2 for more details).

After 10.67 Ma, we infer a decrease in the surface ocean nutrient availability based on the calcareous nannofossil assemblage. This is further supported by a change in the δ^{13}C benthic stack at this time (Westerhold et al., 2020; Figure 6-7), which is indicative of a shift in the C cycle and nutrient availability (De Vleeschouwer et al., 2025), as well as a progressive increase in the Shannon diversity index (Figure 2). However, both the global benthic δ^{18}O (Westerhold et al., 2020) and estimations of the westerlies position for this time period indicate stable conditions in the Antarctic region that lasted until ~10 Ma (Groeneveld et al., 2017). In this regard, we point out that the enhancement of the Tasman Leakage at this time, which transports warm and nutrient-depleted waters from the Pacific Ocean, could be responsible for the decrease in surface ocean nutrient availability (Lyu et al., 2023; De Vleeschouwer et al., 2025). Lyu et al. (2023) established the beginning of the Tasman Leakage at ~11 Ma, based on an increase in grain size and winnowing currents at ODP Site 752. This is further supported by a decrease in the dust flux index at this same time, potentially due to winnowing (Figure 6).

Furthermore, εNd(t) data from Site 707 and 752 show an increasing trend after 11 Ma, which is indicative of higher Pacific Ocean water input into the Indian Ocean (Figure 6). However, its effect on the surface ocean remained limited until 10.67 Ma. This condition persisted until 9.88 Ma, which is consistent with an intensification of the ACC and a subsequent increase in the northward water transport (Holbourn et al., 2013; Evangelinos et al., 2024; De Vleeschouwer et al., 2025).

An increase in the nutrient availability was recorded after 9.22 Ma, indicating an intensification of the Antarctic lateral transport (Figure 7C). This increase in productivity is further supported by the Shannon diversity index, which shows a sharp decrease at this time (Figure 2). Interestingly, within this period, we recorded an increase of small-sized reticulofenestrids (8.95-8.71 Ma), which have been ascribed in the literature to variations in the N:P ratio (Müller et al., 2008; Aloisi, 2015). This is further supported by benthic δ^{13}C data obtained at Site 752, which shows no variations during this period. Based on the inferred intensification of the Antarctic lateral transport, we hypothesise that this caused a period of N depletion in the ocean, due to N consumption and remineralisation, which promoted the bloom of r-selected species (such as *R. minuta*).

4.4 Global-scale implications on the nutrient cycling

Our calcareous nannofossil records allowed us to infer a relation between the Antarctic region and the nutrient pool at ODP Site 752. However, the interpreted variations in the Antarctic divergence zone could also have a wider global impact on the nutrient cycle across oceanic basins. We hypothesise that the northward/southward movements of the Antarctic downwelling zone during the Miocene led to a redistribution of the vertical nutrient profile across the different oceanic basins. Specifically, our data suggest that during warm periods,

https://doi.org/10.5194/egusphere-2026-3191
Preprint. Discussion started: 12 June 2026

when the Antarctic divergence zone is located further south, nutrients would be concentrated in the deep waters, reducing surface lateral transport and enhancing productivity in upwelling regions. Meanwhile, as the Antarctic divergence zone migrates north during colder climate conditions, the ocean suffers a decrease in deep-water nutrient trapping and an increase in surface lateral transport, weakening productivity in the upwelling regions and enhancing it in the open ocean. This hypothesis is supported by different studies performed in upwelling and open ocean regions, which observed this same trend (Krammer et al., 2006; Imai et al., 2015, 2020; Hendericks et al., 2020; Auer et al., 2023).

5 Conclusion

In this study, we present a fully quantitative calcareous nannofossil assemblage data set for Site 752. The evaluation of our novel data within a multi-proxy approach permitted us to disentangle the variations in surface oceanic conditions in the Broken Ridge region and related mechanisms during the Middle to Late Miocene. Here, we show that the surface ocean in this region is shaped primarily by global climate via nutrient transport efficiency from the Antarctic divergence and surface water temperature. Furthermore, we observed that variations in coccolith size are deeply connected with nutrient availability. We therefore infer the following conclusions.

1) The combination of calcareous nannofossil data with a multiproxy approach indicates that the Broken Ridge region has been susceptible to multiple paleoceanographic changes during the Middle to Late Miocene (~16.1 – 7.31 Ma) related to shifts in the nutrient availability, water temperature, and stratification. Specifically, we detected 5 intervals and 5 subintervals where the above-mentioned parameters changed.

2) High global temperatures during the MCO resulted in an enhancement of the seasonal signal at the BR. The subsequent decrease in temperatures across the MMCT led to a deepening of the mixed layer and an increase in nutrient availability in the surface waters. This trend continued along the Late Miocene Cooling, reaching the coldest and higher nutrient conditions during Interval 5a. Interestingly, during Interval 5a (10.67–9.88 Ma), a decrease in nutrient availability and an increase in water temperature were recorded, coinciding with an enhanced influx of Pacific Ocean waters into the BR region.

3) The increase in abundance of *R. minuta* recorded at ODP Site 752 during interval 5b is synchronous with that observed in other oceanic areas. We suggest that the increase in abundance of small-sized reticulofenestrids during this time is related to a shift in the N:P ratio and, specifically, points to a variation in the N cycle as a potential driver for this change.

4) Calcareous nannofossil-based shifts in the surface ocean nutrient availability at ODP Site 752 permitted us to elucidate the temporal evolution of the Antarctic divergence region during the Middle to Late Miocene. Specifically, our results revealed a consistent northward migration of the Antarctic divergence region after the MCO that continued up to at least 7.34 Ma. This migration resulted in a major reorganisation of the nutrient cycle in the Indian Ocean.

Appendix 1

https://doi.org/10.5194/egusphere-2026-3191
Preprint. Discussion started: 12 June 2026

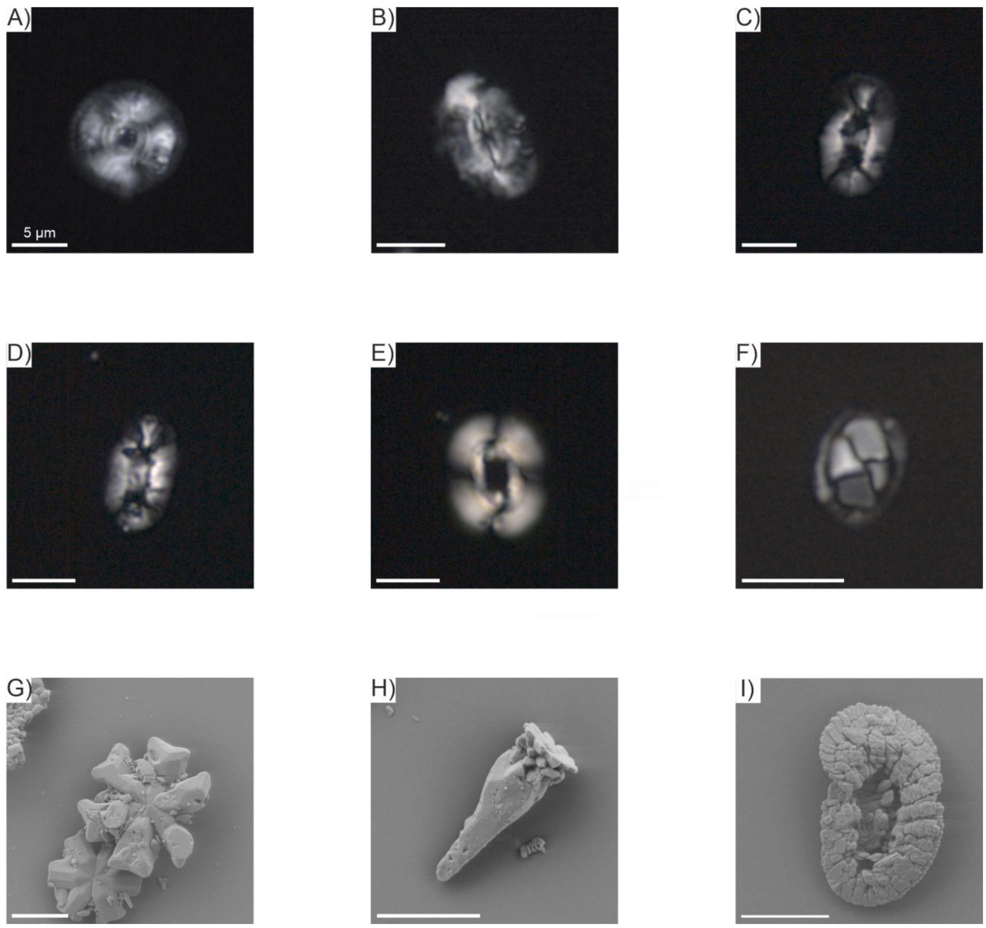

Plate 1: Light microscope and Scanning Electron Microscope images of nannofossil specimens from ODP Site 752. **A)** *Calcidiscus macyntirei* (4H-3W-57-59 cm). **B)** Unidentified specimen (4H-3W-147-149 cm). **C)** *Helicosphaera intermedia* (4H-4W-147-149 cm). **D)** *Helicosphaera* sp. (4H-4W-147-149 cm). **E)** *Reticulofenestra pseudoumbilicus* (4H-4W-147-149 cm). **F)** *Tetralithoides symeonidesii* (4H-4W-147-149 cm). **G)** *Discoaster* sp. (4H-6W-87-89 cm). **H)** *Sphenolithus heteromorphus* (7H-3W-27-29 cm). **I)** *Helicosphaera* sp. (8H-1W-47-49 cm).

Data availability

Data is available from the supplements and on PANGEA.

Competing interests

The contact author has declared that none of the authors has any competing interests.

Acknowledgements

This research used samples and data provided by the International Ocean Discovery Program and its predecessor, the Ocean Drilling Program (ODP). We thank all scientific participants and crew of ODP Leg 121 for making this study possible. This study uses data generated during ReC23-01, a workshop within the Repository Core Re-Discovery Program (ReCoRD) framework, a collaborative program between Kochi Core Center and J-DESC. This research was funded by the Austrian Science Fund (FWF) [Grant DOI: 10.55776/P36046] awarded to GA. For the purpose of open access, the authors have applied a CC BY public copyright licence to any Author Accepted Manuscript version arising from this submission. The German Research Foundation (DFG) provided funding through Project 446900747 (VL96/3-1) awarded to DDV. AVDG was partially funded by the Alexander von Humboldt Research Fellowship (Henriette-Herz Program).

References

Aloisi, G.: Covariation of metabolic rates and cell size in coccolithophores, Biogeosciences, 12 (15), 4665–4692. https://doi.org/10.5194/bg-12-4665-2015, 2015.

Álvarez, M., Tanhua, T., Brix, H., Lo Monaco, C., Metzl, N., McDonagh, E. L., and Bryden, H. L.: Decadal biogeochemical changes in the subtropical Indian Ocean associated with Subantarctic Mode Water, J. Geophys. Res.- Oceans, 116 (9), 1–13. https://doi.org/10.1029/2010JC006475, 2011.

Aubry, M. P.: Handbook of Cenozoic Calcareous Nannoplankton, Book 1: Ortholithae (Discoasters), Micropaleontology Press, American Museum of Natural History, New York, 266 pp., 1984.

Aubry, M. P.: Handbook of Cenozoic Calcareous Nannoplankton, Book 2: Ortholithae (Catinasters, Ceratoliths, Rhabdoliths), Micropaleontology Press, American Museum of Natural History, New York, 279 pp., 1988.

Aubry, M. P.: Handbook of Cenozoic Calcareous Nannoplankton, Book 3: Ortholithae (Pentaliths, and others) Heliolithae (Fasciculiths, Sphenoliths and others), Micropaleontology Press, American Museum Natural History, New York, 279 pp., 1989.

Aubry, M. P.: Handbook of Cenozoic Calcareous Nannoplankton, Book 4: Heliolithae (Helicoliths, Cribriliths, Lopadoliths and others), Micropaleontology Press, American Museum of Natural History, New York, 381 pp., 1990.

Aubry, M.-P.: Handbook of Cenozoic Calcareous Nannoplankton, Book 5: Heliolithae (Zygoliths and Rhabdoliths), Micropaleontology Press, American Museum of Natural History, New York, 368 pp., 1999.

Auer, G., Piller, W. E., and Harzhauser, M.: High-resolution calcareous nannoplankton palaeoecology as a proxy for small-scale environmental changes in the Early Miocene, Mar. Micropaleontol., 111, 53–65, https://doi.org/10.1016/j.marmicro.2014.06.005, 2014.

Auer, G., Piller, W. E., and Harzhauser, M.: Two distinct decadal and centennial cyclicities forced marine upwelling intensity and precipitation during the late Early Miocene in central Europe, Clim. Past, 11, 283–303, https://doi.org/10.5194/cp-11-283-2015, 2015.

Auer, G., De Vleeschouwer, D., Smith, R. A., Bogus, K., Groeneveld, J., Grunert, P., Castañeda, I. S., Petrick, B., Christensen, B., Fulthorpe, C., Gallagher, S. J., and Henderiks, J.: Timing and Pacing of Indonesian Throughflow Restriction and Its Connection to Late Pliocene Climate Shifts, Paleoceanogr. Paleocl., 34, 635–657, https://doi.org/10.1029/2018pa003512, 2019.

Auer, G., Petrick, B., Yoshimura, T., Mamo, B. L., Reuning, L., Takayanagi, H., De Vleeschouwer, D., and Martinez-Garcia, A.: Intensified organic carbon burial on the Australian shelf after the

https://doi.org/10.5194/egusphere-2026-3191
Preprint. Discussion started: 12 June 2026

Middle Pleistocene transition, Quat. Sci. Rev., 262, 106965, https://doi.org/10.1016/j.quascirev.2021.106965, 2021.

Auer, G., Bialik, O. M., Antoulas, M. E., Vogt-Vincent, N., and Piller, W. E.: Biotic response of plankton communities to Middle to Late Miocene monsoon wind and nutrient flux changes in the Oman margin upwelling zone, Clim. Past, 19 (11), 2313–2340, https://doi.org/10.5194/cp-19-2313-2023, 2023.

Bali, H., Gupta, A. K., Joseph, S., and Kaushik, A.: (2025). Exploring the deep water mass turnovers in the Eastern Indian Ocean since the late Oligocene: Significance of ocean gateways and paleoclimate, Palaeogeogr. Palaeoclimatol. Palaeoecol., 657, 112607, https://doi.org/10.1016/j.palaeo.2024.112607, 2025.

Båtvik, H., Heimdal, B. R., Fagerbakke, K. M., and Green, J. C.: Effects of unbalanced nutrient regime on coccolith morphology and size in emiliania huxleyi (prymnesiophyceae), Eur. J. Phycol., 32 (2), 155–165, https://doi.org/10.1080/09670269710001737089, 1997.

Beltran, C., Rouselle, G., Backman, J., Wade, B. S., and Sicre, M. A.: Miocene in the eastern equatorial Pacfic, Paleoceanogr. Paleocl., 29, 210–222, https://doi.org/10.1002/2013PA002506, 2014

Betzler, C., Eberli, G. P., Lüdmann, T., Reolid, J., Kroon, D., Reijmer, J. J. G., Swart, P. K., Wright, J., Young, J. R., Alvarez-Zarikian, C., Alonso-García, M., Bialik, O. M., Blättler, C. L., Guo, J. A., Haffen, S., Horozal, S., Inoue, M., Jovane, L., Lanci, L., Laya, J. C., Hui Mee, A. L., Nakakuni, M., Nath, B. N., Niino, K., Petruny, L. m., Pratiwi, S. D., Slagle, A. L., Sloss, C. R., Su, X., and Yao, Z.: Refinement of Miocene sea level and monsoon events from the sedimentary archive of the Maldives (Indian Ocean), Prog. Earth Planet. Sci., 5 (1), https://doi.org/10.1186/s40645-018-0165-x, 2018.

Bialik, O. M., Frank, M., Betzler, C., Zammit, R., and Waldmann, N. D. (2019). Two-step closure of the Miocene Indian Ocean Gateway to the Mediterranean, Sci. Rep., 9 (1), 1–10, https://doi.org/10.1038/s41598-019-45308-7, 2019.

Bialik, O. M., Auer, G., Ogawa, N. O., Kroon, D., Waldmann, N. D., and Ohkouchi, N.: Monsoons, Upwelling, and the Deoxygenation of the Northwestern Indian Ocean in Response to Middle to Late Miocene Global Climatic Shifts, Paleoceanogr. Paleocl., 35 (2), e2019PA003762, https://doi.org/10.1029/2019PA003762, 2020.

Bialik, O. M., Jarochowska, E., and Grossowicz, M.: Ordination analysis in sedimentology, geochemistry and palaeoenvironment—Background, current trends and recommendations, Depos. Record, 7 (3), 541–563, https://doi.org/10.1002/dep2.161, 2021.

Boesiger, T. M., de Kaenel, E., Bergen, J. A., Browning, E., and Blair, S. A.: Oligocene to Pleistocene taxonomy and stratigraphy of the genus Helicosphaera and other placolith taxa in the circum North Atlantic Basin, J. Nannoplankton Res., 37 (2–3), 145–175, https://doi.org/10.58998/jnr2021, 2017.

Böning, P., and Bard, E.: Millennial/centennial-scale thermocline ventilation changes in the Indian Ocean as reflected by aragonite preservation and geochemical variations in Arabian Sea sediments, Geochim. Cosmochim. Ac., 73 (22), 6771–6788, https://doi.org/10.1016/j.gca.2009.08.028, 2009.

https://doi.org/10.5194/egusphere-2026-3191
Preprint. Discussion started: 12 June 2026

Bordiga, M., Bartol, M., and Henderiks, J.: Absolute nannofossil abundance estimates: Quantifying the pros and cons of different techniques, Rev. Micropaleontol., 58 (3), 155–165, https://doi.org/10.1016/j.revmic.2015.05.002, 2015.

Bown, P. R., and Dunkley Jones, T.: Calcareous nannofossils from the Paleogene equatorial Pacific (IODP Expedition 320 Sites U1331-1334), J. Nannoplankton Res., 32 (2), 3–51, https://doi.org/10.58998/jnr2023, 2012

Browning, E., Bergen, J. A., Blair, S. A., Boesiger, T. M., and de Kaenel, E.: Late Miocene to Late Pliocene taxonomy and stratigraphy of the genus Discoaster in the circum North Atlantic Basin: Gulf of Mexico and ODP Leg 154, J. Nannoplankton Res., 37 (2–3), 189–214, https://doi.org/10.58998/jnr2037, 2017

Bukry, D., and Percival Jr, S. F.: New Tertiary calcareous nannofossils, Tulane Studies in Geology and Paleontology, 8, 123–146, 1971

Burke, K. D., Williams, J. W., Chandler, M. A., Haywood, A. M., Lunt, D. J., and Otto-Bliesner, B. L.: Pliocene and Eocene provide best analogs for near-future climates, PNAS, 115(52), 13288–13293, https://doi.org/10.1073/pnas.1809600115, 2018

Burton, L. E., Oldeman, A. M., Haywood, A. M., Tindall, J. C., Dolan, A. M., Hill, D. J., von der Heydt, A., and Baatsen, M. L. J.: An assessment of the Pliocene as an analogue for our warmer future, Glob. Planet. Change, 252, 104860, https://doi.org/10.1016/j.gloplacha.2025.104860, 2025.

Buzas M.A., and Gibson, T.G.: Species diversity: benthonic foraminifera in western North Atlantic, Science, 163 ,3862, 72-75, https://doi.org/10.1126/science.163.3862.72, 1969.

Cachão, M., and Moita, M. T.: Coccolithus pelagicus, a productivity proxy related to moderate fronts off Western Iberia, Mar. Micropaleontol., 39 (1–4), 131–155, https://doi.org/10.1016/S0377-8398(00)00018-9, 2000.

Chakraborty, A., Ghosh, A. K., Dey, R., Saxena, S., and Mazumder, A.: Record of the Miocene Climate Optimum in the northeast Indian Ocean: evidence from the microfossils, Palaeobiodiversity Palaeoenvironments, 99 (2), 159–175, https://doi.org/10.1007/s12549-018-0342-3, 2018.

Chelton, D. B., and Xie, S. P.: Coupled ocean-atmosphere interaction at oceanic mesoscales, Oceanography, 23 (4), 54–69, https://doi.org/10.5670/oceanog.2010.05, 2010.

Costanza, R.: The ecological, economic, and social importance of the oceans, Ecol. Econ., 31 (2), 199–213, https://doi.org/10.1016/S0921-8009(99)00079-8, 1999.

Dankel, D. J., Aasly, K., Carić, H., Ellefmo, S. L., Gaspers, A., Hixson, R., Lloret, J., Oftebro, T. L., Sowman, G. J., and Cowan, E.: Ocean sectors: Case studies of human activity in the Ocean-based economy, in: Oceans and Human Health, edited by: Fleming, L. E., Alcantara Creencia, L. B., Gerwick, W. H., Goh, H. C., Gribble, M. O., Maycock, B., Solo-Gabriele, H., Academic Press, 531–546, https://doi.org/10.1016/B978-0-323-95227-9.00014-2, 2023.

De Vleeschouwer, D., Drury, A. J., Vahlenkamp, M., Rochholz, F., Liebrand, D., and Pälike, H.: High-latitude biomes and rock weathering mediate climate–carbon cycle feedbacks on eccentricity timescales. Nat. Commun., 11 (1), 1–10. https://doi.org/10.1038/s41467-020-18733-w, 2020.

De Vleeschouwer, D., Lyu, J., Bialik, O. M., Christensen, B. A., Auer, G., and Batenburg, S. J.: Pacific-Indian Ocean Intermediate Water Exchange Since the Middle Miocene: From Indonesian Throughflow to Tasman Leakage, Paleoceanogr. Paleocl., 40 (9), e2025PA005169, https://doi.org/10.1029/2025PA005169, 2025.

Deutsch, C., Sarmiento, J. L., Sigman, D. M., Gruber, N., and Dunne, J. P.: Spatial coupling of nitrogen inputs and losses in the ocean, Nature, 445 (7124), 163–167, https://doi.org/10.1038/nature05392, 2007.

Dexter, E., Rollwagen-Bollens, G., and Bollens, S. M.: The trouble with stress: A flexible method for the evaluation of nonmetric multidimensional scaling, Limnol. Oceanogr.: Methods, 16 (7), 434–443, https://doi.org/10.1002/lom3.10257, 2018

Efron, B., and Tibshirani, R.J.: An Introduction to the Bootstrap (1st ed.), Chapman and Hall/CRC, https://doi.org/10.1201/9780429246593, 1994.

Evangelinos, D., Etourneau, J., van de Flierdt, T., Crosta, X., Jeandel, C., Flores, J. A., Harwood, D. M., Valero, L., Ducassou, E., Sauermilch, I., Klocker, A., Cacho, I., Pena, L. D., Kreissig, K., Benoit, M., Belhadj, M., Paredes, E., Garcia-Solsona, E., López-Quirós, A., Salabarnada, A., and Escutia, C.: Late Miocene onset of the modern Antarctic Circumpolar Current, Nat. Geosci., 17 (2), 165–170, https://doi.org/10.1038/s41561-023-01356-3, 2024.

Feely, R. A., Sabine, C. L., Schlitzer, R., Bullister, J. L., Mecking, S., and Greeley, D.: Oxygen utilizatiuon and organic carbon remineralization in the upper water column of the Pacific Ocean, J. Oceanogr., 60 (1), 45–52, https://doi.org/10.1023/B:JOCE.0000038317.01279.aa, 2004.

Fox, L. R., Wade, B., Holbourn, A., Leng, M. J., and Bhatia, R.: Temperature gradients across the Pacific Ocean during the Middle Miocene, Paleoceanogr. Paleocl., 36 (6), e2020PA003924, https://doi.org/10.1029/2020PA003924, 2021.

Galović, I., and Young, J.: Revised taxonomy and stratigraphy of Middle Miocene calcareous nannofossils of the Paratethys, Micropaleontology, 58 (4), 305–334, https://doi.org/10.47894/mpal.58.4.01, 2012.

Garcia-Soto, C., Cheng, L., Caesar, L., Schmidtko, S., Jewett, E. B., Cheripka, A., Rigor, I., Caballero, A., Chiba, S., Báez, J. C., Zielinski, T., and Abraham, J. P.: An Overview of Ocean Climate Change Indicators: Sea Surface Temperature, Ocean Heat Content, Ocean pH, Dissolved Oxygen Concentration, Arctic Sea Ice Extent, Thickness and Volume, Sea Level and Strength of the AMOC (Atlantic Meridional Overturning Circulation), Front. Mar. Sci., 8, 642372 , https://doi.org/10.3389/fmars.2021.642372, 2021.

Groeneveld, J., Henderiks, J., Renema, W., McHugh, C. M., De Vleeschouwer, D., Christensen, B. A., Fulthorpe, C. S., Reuning, L., Gallagher, S. J., Bogus, K., Auer, G., and Ishiwa, T.: Australian shelf sediments reveal shifts in Miocene Southern Hemisphere westerlies, Sci. Adv., 3 (5), 1–8, https://doi.org/10.1126/sciadv.1602567, 2017.

Hallock, P.: Fluctuations in the trophic resource continuum: A factor in global diversity cycles?, Paleoceanogr. Paleocl., 2 (5), 457–471, https://doi.org/10.1029/PA002i005p00457, 1987.

Hammer, Ø. and Harper, D. A. T.: Paleontological Data Analysis, 1st ed., Blackwell Publishing Ltd, ISBN 9781405115445, 2006.

https://doi.org/10.5194/egusphere-2026-3191
Preprint. Discussion started: 12 June 2026

Hammer, Ø., Harper, D. A. T., and Ryan, P. D.: PAST: Paleontological Statistics software package for education and data analysis, Palaeontol. Electron., 4 (1), 1–9, http://palaeo-electronica.org/2001_1/past/issue1_01.htm, 2001.

Hamon, N., Sepulchre, P., Lefebvre, V., and Ramstein, G.: The role of eastern Tethys seaway closure in the Middle Miocene Climatic Transition (ca. 14 Ma), Clim. Past, 9 (6), 2687–2702, https://doi.org/10.5194/cp-9-2687-2013, 2013.

Hanawa, K., and L. D. Talley: Mode waters, in: Ocean Circulation and Climate, vol. 77, International Geophysics Series, edited by: Siedler,G., Church, J., and Gould, J., 373–386, Academic Press, New York, 2001.

Haq, B. U.: Biogeographic history of Miocene calcareous nannoplankton and paleoceanography of the Atlantic Ocean, Micropaleontology, 26 (4), 414–443, https://doi.org/10.2307/1485353, 1980.

Harms, N. C., Lahajnar, N., Gaye, B., Rixen, T., Dähnke, K., Ankele, M., Schwarz-Schampera, U., and Emeis, K.-C.: Nutrient distribution and nitrogen and oxygen isotopic composition of nitrate in water masses of the subtropical southern Indian Ocean, Biogeosciences, 16 (13), 2715–2732, https://doi.org/10.5194/bg-16-2715-2019, 2019.

Hartin, C. A., Fine, R. A., Kamenkovich, I., and Sloyan, B. M.: Comparison of Subantarctic Mode Water and Antarctic Intermediate Water formation rates in the South Pacific between NCAR-CCSM4 and observations, Geophys. Res. Lett., 41 (2), 519–526, https://doi.org/10.1002/2013GL058728, 2014.

Hauck, J., Völker, C., Wolf-Gladrow, D. A., Laufkötter, C., Vogt, M., Aumont, O., Bopp, L., Buitenhuis, E. T., Doney, S. C., Dunne, J., Gruber, N., Hashioka, T., John, J., Quéré, C. Le, Lima, I. D., Nakano, H., Séférian, R., and Totterdell, I.: On the Southern Ocean CO_2 uptake and the role of the biological carbon pump in the 21st century, Global Biogeochemical Cycles, 29 (9), 1451–1470, https://doi.org/10.1002/2015GB005140, 2015.

Henderiks, J., Bartol, M., Pige, N., Karatsolis, B. T., and Lougheed, B. C.: Shifts in Phytoplankton Composition and Stepwise Climate Change During the Middle Miocene, Paleoceanogr. Paleocl., 35 (8), e2020PA003915, https://doi.org/10.1029/2020PA003915, 2020.

Henry, M., and Vallis, G. K.: Variations on a Pathway to an Early Eocene Climate, Paleoceanogr. Paleocl., 37 (8), e2021PA004375, https://doi.org/10.1029/2021PA004375, 2022.

Herbert, T. D., Lawrence, K. T., Tzanova, A., Peterson, L. C., Caballero-Gill, R., and Kelly, C. S.: Late Miocene global cooling and the rise of modern ecosystems. Nat. Geosci., 9 (11), 843–847. https://doi.org/10.1038/ngeo2813, 2016.

Holbourn, A., Kuhnt, W., Lyle, M., Schneider, L., Romero, O., and Andersen, N.: Middle Miocene climate cooling linked to intensifi cation of eastern equatorial Pacifi c upwelling, Geology, 42(1), 19–22, https://doi.org/10.1130/G34890.1, 2013.

Holbourn, A., Kuhnt, W., Kochhann, K., Andersen, N., and MAtsuzaki, K. M.: Keys for understanding future trends on a warmer Earth ?, in: Understanding the Monterey Formation and Similar Biosiliceous Units across Space and Time, edited by: Aiello, I. W., Barron, J. A., Ravelo, A. C., Geol. Soc. Am., Spec. Pap., 2556 (05), 1–20, https://doi.org/10.1130/2022.2556(05), 2022.

Howe, R.: Ultrastructure and taxonomy of the family Sphenolithaceae, J. Nannoplankton Res., 39 (1), 29–75, https://doi.org/10.58998/jnr2124, 2021.

Imai, R., Farida, M., Sato, T., and Iryu, Y.: Evidence for eutrophication in the northwestern Pacific and eastern Indian oceans during the Miocene to Pleistocene based on the nannofossil accumulation rate, Discoaster abundance, and coccolith size distribution of Reticulofenestra, Mar. Micropaleontol., 116, 15–27, https://doi.org/10.1016/j.marmicro.2015.01.001, 2015.

Imai, R., Sato, T., Chiyonobu, S., and Iryu, Y.: Reconstruction of Miocene to Pleistocene sea-surface conditions in the eastern Indian Ocean on the basis of calcareous nannofossil assemblages from ODP Hole 757B. Island Arc, 29 (1), e12373, https://doi.org/10.1111/iar.12373, 2020.

Jo, A. R., Lee, J. Y., Timmermann, A., Jin, F. F., Yamaguchi, R., and Gallego, A.: Future Amplification of Sea Surface Temperature Seasonality Due To Enhanced Ocean Stratification, Geophys. Res. Lett., 49 (9), 1–10, https://doi.org/10.1029/2022GL098607, 2022.

Kageyama, M., Braconnot, P., Chiessi, C. M., Rehfeld, K., Ait Brahim, Y., Dütsch, M., Gwinneth, B., Hou, A., Loutre, M. F., Hendrizan, M., Meissner, K., Mongwe, P., Otto-Bliesner, B., Pezzi, L. P., Rovere, A., Seltzer, A., Sime, L., and Zhu, J.: Lessons from paleoclimates for recent and future climate change: opportunities and insights, Front. Clim., 6, 1511997, https://doi.org/10.3389/fclim.2024.1511997, 2024.

Klotz, S., Fauquette, S., Combourieu-Nebout, N., Uhl, D., Suc, J. P., and Mosbrugger, V.: Seasonality intensification and long-term winter cooling as a part of the Late Pliocene climate development, Earth Planet. Sci. Lett., 241 (1–2), 174–187, https://doi.org/10.1016/j.epsl.2005.10.005, 2006.

Koch-Larrouy, A., Morrow, R., Penduff, T., and Juza, M.: Origin and mechanism of Subantarctic Mode Water formation and transformation in the Southern Indian Ocean, Ocean Dyn., 60 (3), 563–583, https://doi.org/10.1007/s10236-010-0276-4, 2010.

Koehn, J. Z., Allison, E. H., Franz, N., and Wiegers, E. S.: How Can the Oceans Help Feed 9 Billion People? In: Conservation for the Anthropocene Ocean, edited by: Levin, P. S., and Poe, M. R., Elsevier Inc, 65-88, https://doi.org/10.1016/B978-0-12-805375-1.00004-0, 2017.

Krammer, R., Baumann, K. H., and Henrich, R.: Middle to late Miocene fluctuations in the incipient Benguela Upwelling System revealed by calcareous nannofossil assemblages (ODP Site 1085A), Palaeogeogr. Paleocl., 230 (3–4), 319–334, https://doi.org/10.1016/j.palaeo.2005.07.022, 2006.

Kraus, E. B., and Businger, J. A.: Atmosphere-Ocean Interaction (2nd ed., p. 362), Oxford University Press, 1994.

Kuhnt, W., Holbourn, A., Xu, J., Opdyke, B., De Deckker, P., Röhl, U., and Mudelsee, M.: Southern Hemisphere control on Australian monsoon variability during the late deglaciation and Holocene, Nat. Commun., 6, 5916, https://doi.org/10.1038/ncomms6916, 2015.

Langer, G., Jie, V. W., Kottmeier, D., Flori, S., Sturm, D., de Vries, J., Harper, G. M., Brownlee, C., and Wheeler, G.: Distinct physiological responses of Coccolithus braarudii life cycle phases to light intensity and nutrient availability, Eur. J. Phycol., 58 (1), 58–71. https://doi.org/10.1080/09670262.2022.2056925, 2023.

https://doi.org/10.5194/egusphere-2026-3191
Preprint. Discussion started: 12 June 2026

Laufkötter, C., Vogt, M., Gruber, N., Aumont, O., Bopp, L., Doney, S. C., Dunne, J. P., Hauck, J., John, J. G., Lima, I. D., Seferian, R., and Völker, C.: Projected decreases in future marine export production: The role of the carbon flux through the upper ocean ecosystem, Biogeosciences, 13(13), 4023–4047, https://doi.org/10.5194/bg-13-4023-2016, 2016.

Laufkötter, C., and Gruber, N.: Will marine productivity wane?, Science, 359 (6380), 1103–1104, https://doi.org/10.1126/science.aat0795, 2018.

Lefèvre, D., Denis, M., Lambert, C. E., and Miquel, J. C.: Is DOC the main source of organic matter remineralization in the ocean water column?, J. Mar. Syst., 7 (2–4), 281–291, https://doi.org/10.1016/0924-7963(95)00003-8, 1996.

Li, Z., England, M. H., Groeskamp, S., Cerovečki, I., and Luo, Y.: The Origin and Fate of Subantarctic Mode Water in the Southern Ocean, J. Phys. Oceanogr., 2951–2972, https://doi.org/10.1175/JPO-D-20-0174.1, 2021.

Lohmann, G. P., and Carlson, J. J.: Oceanographic significance of Pacific late miocene calcareous nannoplankton, Mar. Micropaleontol., 6 (5–6), 553–579, https://doi.org/10.1016/0377-8398(81)90021-9, 1981.

Lyu, J., Auer, G., Bialik, O. M., Christensen, B., Yamaoka, R., and De Vleeschouwer, D.: Astronomically-Paced Changes in Paleoproductivity, Winnowing, and Mineral Flux Over Broken Ridge (Indian Ocean) Since the Early Miocene, Paleoceanogr. Paleocl., 38 (12), e2023PA004761, https://doi.org/10.1029/2023PA004761, 2023.

Mahadevan, A., and Archer, D.: Modeling the impact of fronts and mesoscale circulation on the nutrient supply and biogeochemistry of the upper ocean, J. Geophys. Res.- Oceans, 105 (C1), 1209–1225, https://doi.org/10.1029/1999jc900216, 2000.

Majewski, W.: Mid-Miocene invasion of ecological niches by planktonic foraminifera of the Kerguelen Plateau, Antarctica, Mar. Micropaleontol., 46 (1–2), 59–81, https://doi.org/10.1016/S0377-8398(02)00051-8, 2002.

Marañón, E., Cermeño, P., López-Sandoval, D. C., Rodríguez-Ramos, T., Sobrino, C., Huete-Ortega, M., Blanco, J. M., and Rodríguez, J.: Unimodal size scaling of phytoplankton growth and the size dependence of nutrient uptake and use, Ecol. Lett., 16(3), 371–379, https://doi.org/10.1111/ele.12052, 2013.

Martinot, C., Bolton, C. T., Sarr, A. C., Donnadieu, Y., Garcia, M., Gray, E., and Tachikawa, K.: Drivers of Late Miocene Tropical Sea Surface Cooling: A New Perspective From the Equatorial Indian Ocean, Paleoceanogr. Paleocl., 37 (10), e2024AV001356, https://doi.org/10.1029/2021PA004407, 2022.

McCartney, M. S.,: Antarctic mode water, in: A Voyage of Discovery: George Deacon 70th Anniversary Volume,edited by: Angel, M. V., Pergamon Press, (pp. 103–119), 1977.

McCartney, M. S.,: The subtropical recirculation of mode water, J. Mar. Res., 40, 427–464, 1982.

Mello, J. F., and Buzas, M.: An Application of Cluster Analysis as a Method of Determining Biofacies,J. Paleontol., 42 (3), 747–758, 1968.

https://doi.org/10.5194/egusphere-2026-3191
Preprint. Discussion started: 12 June 2026

Moore, C. M., Mills, M. M., Langlois, R., Milne, A., Achterberg, E. P., La Roche, J., and Geider, R. J.: Relative influence of nitrogen and phosphorus availability on phytoplankton physiology and productivity in the oligotrophic sub-tropical North Atlantic Ocean, Limnol. Oceanogr., 53 (1), 291–305, https://doi.org/10.4319/lo.2008.53.1.0291, 2008.

Moore, C. M., Mills, M. M., Arrigo, K. R., Berman-Frank, I., Bopp, L., Boyd, P. W., Galbraith, E. D., Geider, R. J., Guieu, C., Jaccard, S. L., Jickells, T. D., La Roche, J., Lenton, T. M., Mahowald, N. M., Marañón, E., Marinov, I., Moore, J. K., Nakatsuka, T., Oschlies, A., Saito, M.A., Thingstad, T. F.,, Tsuda, A., and Ulloa, O.: Processes and patterns of oceanic nutrient limitation, Nat. Geosci., 6 (9), 701–710, https://doi.org/10.1038/ngeo1765, 2013.

Moore, K. J., Fu, W., Primeau, F., Britten, G. L., Lindsay, K., Long, M., Doney, S. C., Mahowald, N., Hoffman, F., and Randerson, J. T.: Sustained climate warming drives declining marine biological productivity, Science, 359 (6380), 113–1143, https://doi.org/10.1126/science.aao6379, 2018.

Müller, M. N., Antia, A. N., and LaRoche, J.: Influence of cell cycle phase on calcification in the coccolithophore Emiliania huxleyi, Limnol. Oceanogr., 53, 506–512, https://doi.org/10.4319/lo.2008.53.2.0506, 2008.

Paasche, E.: Roles of nitrogen and phosphorus in coccolith formation in emiliania huxleyi (prymnesiophyceae), Eur. J. Phycol., 33 (1), 33–42, https://doi.org/10.1080/09670269810001736513, 1998.

Palastanga, V., van Leeuwen, P. J., Schouten, M. W., and de Ruijter, W. P. M.: Flow structure and variability in the subtropical Indian Ocean: Instability of the South Indian Ocean countercurrent, J. Geophys. Res.- Oceans, 112 (1), 1–11, https://doi.org/10.1029/2005JC003395, 2007.

Phillips, H. E., Tandon, A., Furue, R., Hood, R., Ummenhofer, C. C., Benthuysen, J. A., Menezes, V., Hu, S., Webber, B., Sanchez-Franks, A., Cherian, D., Shroyer, E., Feng, M., Wijesekera, H., Chatterjee, A., Yu, L., Hermes, J., Murtugudde, R., Tozuka, T., Su, D., Singh, A., Centurioni, L., Prakash, S and Wiggert, J.: Progress in understanding of Indian Ocean circulation, variability, air-sea exchange, and impacts on biogeochemistry, Ocean Science, 17 (6), 1677–1751, https://doi.org/10.5194/os-17-1677-2021, 2021.

Puentes-Jorge, X., Del Gaudio, A. V., Piller, W. E., De Vleeschouwer, D., Lyu, J., Hechemer, T., and Auer, G.: Middle to Late Miocene integrated biostratigraphy and biozonation for the mid-latitude Indian Ocean (ODP Site 752), Newsl. Stratigr., 58 (3), 343–371, https://doi.org/10.1127/nos/2025/0887, 2025.

Püttmann, T., and Mutterlose, J.: Paleoecology of Late Cretaceous Coccolithophores: Insights From the Shallow-Marine Record, Paleoceanogr. Paleocl., 36 (3), e2020PA004161, https://doi.org/10.1029/2020PA004161, 2021.

Rayner, R., Jolly, C., and Gouldman, C.: Ocean observing and the blue economy, Front. Mar. Sci., 6, 1–6, https://doi.org/10.3389/fmars.2019.00330, 2019.

Reagan, J.R., Seidov, D., Wang, Z., Dukhovskoy, D., Boyer, T. P., Locarnini, R. A., Baranova, O. K., Mishonov, A. V., Garcia, H. E., Bouchard, C., Cross, S. L., and Paver, C. R.,: World Ocean Atlas 2023, Volume 2: Salinity, edited by: Mishonov, A., NOAA Atlas NESDIS 90, https://doi.org/10.25923/70qt-9574, 2024.

https://doi.org/10.5194/egusphere-2026-3191
Preprint. Discussion started: 12 June 2026

Rintoul, S. R., and England, M. H.: Ekman transport dominates local air-sea fluxes in driving variability of subantarctic mode water, J. Phys. Oceanogr., 32 (5), 1308–1321, https://doi.org/10.1175/1520-0485(2002)032<1308:ETDLAS>2.0.CO;2, 2002.

Sarmiento, J. L., Slater, R., Barber, R., Bopp, L., Doney, S. C., Hirst, A. C., Kleypas, J., Matear, R., Mikolajewicz, U., Monfray, P., Soldatov, V., Spall, S. A., and Stouffer, R.: Response of ocean ecosystems to climate warming, Global Biogeochemical Cycles, 18 (3), https://doi.org/10.1029/2003GB002134, 2004.

Sato, T., Yuguchi, S., Takayama, T., and Kameo, K.: Drastic change in the geographical distribution of the cold-water nannofossil Coccolithus pelagicus (Wallich) Schiller at 2.74 Ma in the late Pliocene, with special reference to glaciation in the Arctic Ocean, Mar. Micropaleontol., 52 (1–4), 181–193, https://doi.org/10.1016/j.marmicro.2004.05.003, 2004.

Schlitzer, R.: Ocean Data View 5.5.1, https://odv.awi.de (last access:15 October 2025), 2024.

Schott, F. A., Xie, S. P., and McCreary, J. P.: Indian ocean circulation and climate variability, Rev. Geophys., 47 (1), 1–46, https://doi.org/10.1029/2007RG000245, 2009.

Shannon, C. E.: A Mathematical Theory of Communication, Bell System Technical Journal, 27 (3), 379–423, https://doi.org/10.1002/j.1538-7305.1948.tb01338.x, 1948.

Simpson, E. H.: Measurement of Diversity, Nature, 163 (4148), 688–688. https://doi.org/10.1038/163688a0, 1949

Sloyan, B. M., and Rintoul, S. R.: Circulation, renewal, and modification of antarctic mode and intermediate water, J. Phys. Oceanogr., 31(4), 1005–1030, https://doi.org/10.1175/1520-0485(2001)031<1005:CRAMOA>2.0.CO;2, 2001.

Sokal, R. R. and Rohlf, F. J.: Biometry, 3rd ed., W. H. Freeman and Company, ISBN 9780716724117, 1995.

Somerfield, P. J., Clarke, K. R., and Gorley, R. N.: Analysis of similarities (ANOSIM) for 2-way layouts using a generalised ANOSIM statistic, with comparative notes on Permutational Multivariate Analysis of Variance (PERMANOVA), Austral Ecology, 46 (6), 911–926. https://doi.org/10.1111/aec.13059, 2021a.

Somerfield, P. J., Clarke, K. R., and Gorley, R. N.: A generalised analysis of similarities (ANOSIM) statistic for designs with ordered factors, Austral Ecology, 46 (6), 901–910, https://doi.org/10.1111/aec.13043, 2021b.

Sosdian, S. M., and Lear, C. H.,: Initiation of the Western Pacific Warm Pool at the Middle Miocene Climate Transition?, Paleoceanogr. Paleoclimatol., 35, e2020PA003920, https://doi.org/10.1029/2020pa003920, 2020.

Sparrow, M. D., Heywood, K. J., Brown, J., and Stevens, D. P.: Current structure of the south Indian Ocean, J. Geophys. Res.- Oceans, 101 (C3), 6377–6391, https://doi.org/10.1029/95JC03750, 1996.

Steinthorsdottir, M., Jardine, P. E., and Rember, W. C.: Near-Future pCO2 During the Hot Miocene Climatic Optimum, Paleoceanogr. Paleocl., 36 (1), e2020PA003900, https://doi.org/10.1029/2020PA003900, 2020.

https://doi.org/10.5194/egusphere-2026-3191
Preprint. Discussion started: 12 June 2026

Steinthorsdottir, M., Coxall, H. K., de Boer, A. M., Huber, M., Barbolini, N., Bradshaw, C. D., Burls, N. J., Feakins, S. J., Gasson, E., Henderiks, J., Holbourn, A. E., Kiel, S., Kohn, M. J., Knorr, G., Kürschner, W. M., Lear, C. H., Liebrand, D., Lunt, D. J., Mörs, T., Pearson, P. N., Pound, M. J., Stoll, H., and Strömberg, C. A. E.: The Miocene: The Future of the Past, Paleoceanogr. Paleocl., 36 (4), e2020PA004037, https://doi.org/10.1029/2020PA004037, 2021.

Stenseth, N. C., Mysterud, A., Ottersen, G., Hurrell, J. W., Chan, K. S., and Lima, M.: Ecological effects of climate fluctuations, Science, 297 (5585), 1292–1296, https://doi.org/10.1126/science.1071281, 2002.

Stramma, L.: The South Indian Ocean Current, J. Phys. Oceanogr., 22(4), 421–430, https://doi.org/10.1175/1520-0485(1992)022<0421:TSIOC>2.0.CO;2, 1992.

Stramma, L., and Lutjeharms, J. R. E.: The flow field of the subtropical gyre of the South Indian Ocean, J. Geophys. Res.- Oceans, 102 (C3), 5513–5530, https://doi.org/10.1029/96JC03455, 1997.

Super, J. R., Thomas, E., Pagani, M., Huber, M., O'Brien, C., and Hull, P. M.: North Atlantic temperature and pCO_2 coupling in the early-middle Miocene, Geology, 46 (6), 519-522, https://doi.org/10.1130/G40228.1, 2018.

Tangunan, D. N., Baumann, K. H., Just, J., LeVay, L. J., Barker, S., Brentegani, L., De Vleeschouwer, D., Hall, I. R., Hemming, S., and Norris, R.: The last 1 million years of the extinct genus Discoaster: Plio–Pleistocene environment and productivity at Site U1476 (Mozambique Channel), Palaeogeogr. Palaeocl., 505, 187–197, https://doi.org/10.1016/j.palaeo.2018.05.043, 2018.

Teh, L. C. L., Cheung, W. W. L., and Sumaila, R.: Assessing the Economic Contribution of Ocean-Based Activities Using the Pacific Coast of British Columbia as a Case Study, Sustainability, 14 (14), 1–14, https://doi.org/10.3390/su14148662, 2022.

Tierney, J. E., King, J., Osman, M. B., Abell, J. T., Burls, N. J., Erfani, E., Cooper, V. T., and Feng, R.: Pliocene Warmth and Patterns of Climate Change Inferred From Paleoclimate Data Assimilation, AGU Advances, 6 (1), https://doi.org/10.1029/2024AV001356, 2025.

Verducci, M., Foresi, L. M., Scott, G. H., Sprovieri, M., Lirer, F., and Pelosi, N.: The Middle Miocene climatic transition in the Southern Ocean: Evidence of paleoclimatic and hydrographic changes at Kerguelen plateau from planktonic foraminifers and stable isotopes, Palaeogeogr. Palaeocl., 280 (3–4), 371–386, https://doi.org/10.1016/j.palaeo.2009.06.024, 2009.

Viganò, A., Coxall, H. K., Holmström, M., Vinco, M., Lear, C. H., and Agnini, C.: Calcareous nannofossils across the Eocene-Oligocene transition at Site 756 (Ninetyeast Ridge, Indian Ocean): implications for biostratigraphy and paleoceanographic clues, Newsl. Stratigr., 56 (2), 187–223, https://doi.org/10.1127/nos/2022/0725, 2023.

Wade, B. S., and Bown, P. R.: Calcareous nannofossils in extreme environments: The Messinian Salinity Crisis, Polemi Basin, Cyprus, Palaeogeogr. Palaeocl., 233 (3–4), 271–286, https://doi.org/10.1016/j.palaeo.2005.10.007, 2006.

https://doi.org/10.5194/egusphere-2026-3191
Preprint. Discussion started: 12 June 2026

Wang, Y., and Gligorovski, S.: Atmospheric implications of ocean–atmosphere physicochemical interactions, Atmos. Chem. Phys., 25 (19), 11757–11787, https://doi.org/10.5194/acp-25-11757-2025, 2025.

Wei, W. and Wise, S. W.: Middle Eocene to Pleistocene calcareous nannofossils recovered by Ocean Drilling Program Leg 113, in: the Weddell Sea. Proc., Scientific Results, ODP, Leg 113, Weddell Sea, Antarctica, edited by: Barker, P. F., and Kennett, J. P., College Station TX, 113, 639–666, https://doi.org/10.2973/odp.proc.sr.113.125.1990, 1990.

Westerhold, T., Marwan, N., Drury, A. J., Liebrand, D., Agnini, C., Anagnostou, E., Barnet, J. S. K., Bohaty, S. M., De Vleeschouwer, D., Florindo, F., Frederichs, T., Hodell, D. A., Holbourn, A. E., Kroon, D., Lauretano, V., Littler, K., Lourens, L. J., Lyle, M., Pälike, H., Röhl, U., Tian, J., Wilkens, R. H., Wilson, P. A., and Zachos, J. C.: An astronomically dated record of Earth's climate and its predictability over the last 66 million years, Science, 369 (6509), 1383–1388, https://doi.org/10.1126/SCIENCE.ABA6853, 2020.

Whitney, F. A., Crawford, W. R., and Harrison, P. J.: Physical processes that enhance nutrient transport and primary productivity in the coastal and open ocean of the subarctic NE Pacific. Deep-Sea Res. Part II, 52 (5–6), 681–706, https://doi.org/10.1016/j.dsr2.2004.12.023, 2005.

Williams, R. G., and Follows, M. J.: Physical Transport of Nutrients and the Maintenance of Biological Production, Ocean Biogeochemistry, 19–51, https://doi.org/10.1007/978-3-642-55844-3_3, 2003.

Wong, A. P. S., Bindoff, N. L., and Church, J. A.: Large-scale freshening of intermediate waters in the Pacific and Indian oceans, Nature, 400 (6743), 440–443, https://doi.org/10.1038/22733, 1999.

Wyrtki, K.: Physical Oceanography of the Indian Ocean, in: The Biology of the Indian Ocean, edited by: Zeitzschel, B., and Gerlach, S. A., 18–36, https://doi.org/10.1007/978-3-642-65468-8_3, 1973.

You, Y: Intermediate water circulation and ventilation of the Indian Ocean derived from water-mass contributions, Journal of Marine Research 56, 5, https://elischolar.library.yale.edu/journal_of_marine_research/2299, 1998.

Young, J.: Size variation of Neogene Reticulofenestra coccoliths from Indian Ocean DSDP Cores, J. Micropalaeontol., 9, 71–85, https://doi.org/10.1144/jm.9.1.71, 1990.

Young, J. R.: Neogene, in: Calcareous Nannofossil Biostratigraphy, edited by: Bown, P. R., 225–265, ISBN 9780412789700, 1998.

Young, J. R., Bown P. R., and Lees J. A.: Nannotax3 website. International Nannoplankton Association, www.mikrotax.org/Nannotax3 (Last access: 13 August 2025), 2022.